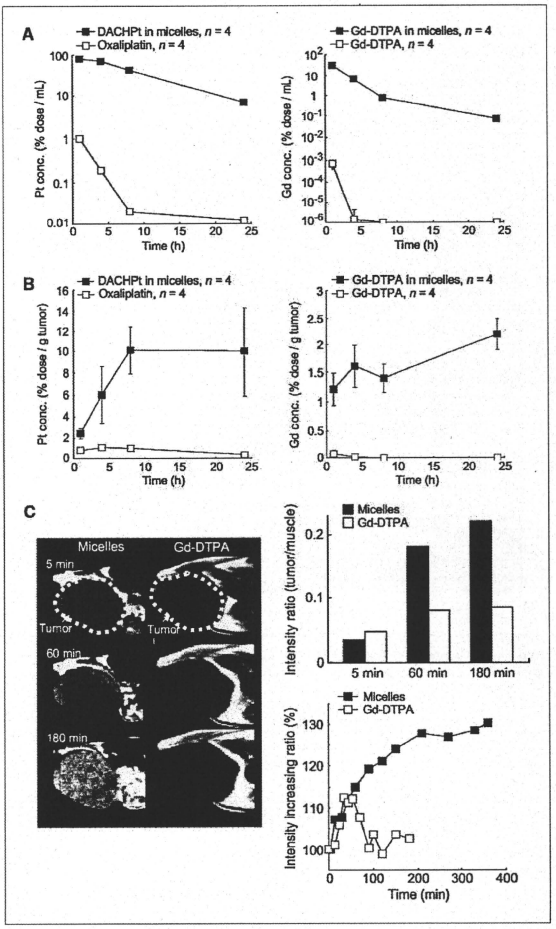

Figure 3. *In vivo* behavior of Gd-DTPA/DACHPt–loaded micelles. A, left, plasma clearance of Pt drugs after i.v. injection of oxaliplatin and Gd-DTPA/DACHPt–loaded micelles; right, plasma clearance of Gd complexes after i.v. injection of Gd-DTPA and Gd-DTPA/DACHPt–loaded micelles. B, left, accumulation of Pt drugs in the C-26 tumor after i.v. injection of oxaliplatin or Gd-DTPA/DACHPt–loaded micelles; right, accumulation of Gd complexes in C-26 tumors after i.v. injection of Gd-DTPA or Gd-DTPA/DACHPt–loaded micelles. C, left, *in vivo* MRI series of T_1-weighted transaxial slices of C-26 subcutaneous tumor after i.v. injection of Gd-DTPA/DACHPt–loaded micelles or Gd-DTPA at 5 μmol/kg Gd-DTPA. Right, top, tumor-to-muscle intensity ratio for the micelles and Gd-DTPA at 5, 60, and 180 min; bottom, relative intensity enhancement in the tumor after i.v. injection of Gd-DTPA/DACHPt–loaded micelles or Gd-DTPA at 5 μmol/kg Gd-DTPA.

distribution of heme proteins. Accordingly, the PECAM-1–positive area from the immunofluorescence microscopy (Fig. 6A) showing the existence of endothelial cells is consistent with this Fe-rich area (Fig. 6B). The K-rich regions possibly correspond to pancreatic cancer cells because K is a cofactor required to obtain maximum activity of the pyruvate kinase, an enzyme involved in glycolytic energy production, which has been observed in carcinoma tissue of the pancreas (31). The Gd as well as the Pt atoms located at those K-rich areas suggest the selective tumor accumulation of Gd-DTPA and DACHPt. Moreover, the colocalization of the Gd-DTPA and DACHPt confirms the high potential of Gd-DTPA/

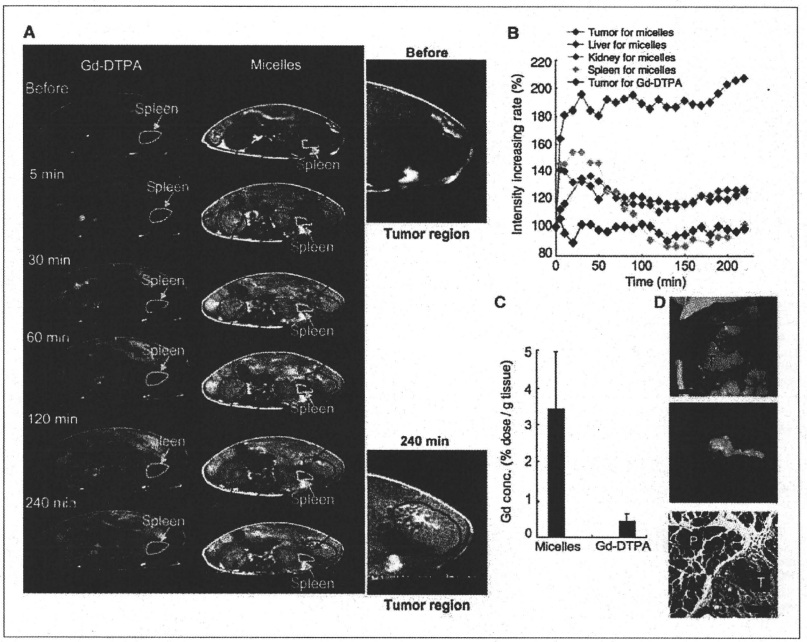

Figure 4. *In vivo* behavior of Gd-DTPA/DACHPt–loaded micelles on an orthotopic pancreatic cancer (BxPC3). A, *in vivo* MRI series of T_1-weighted transaxial slices of mice after i.v. injection of Gd-DTPA/DACHPt–loaded micelles or Gd-DTPA at 5 μmol/kg. B, relative MRI intensity in each organ after i.v. injection of Gd-DTPA/DACHPt–loaded micelles at 5 μmol/kg Gd-DTPA or i.v. injection of Gd-DTPA at 5 μmol/kg. C, the Gd-DTPA/DACHPt–loaded micelles and Gd-DTPA accumulation in the BxPC3 tumor 4 h after i.v. administration (n = 4). D, top, macroscopic findings of orthotopic BxPC3-bearing BALB/c nude mice after MRI acquisition. Scale bar, 1 cm. Pancreatic cancer (T), liver (L), kidney (K), and spleen (S). Middle, the pancreatic tumor after excision with spleen and normal pancreas. Scale bar, 0.5 cm. Bottom, microscopic findings (H&E staining) of the pancreatic cancer (T) and normal pancreatic tissue (P). Scale bar, 100 μm.

DACHPt–loaded micelles to assess the distribution of the anticancer drug at the tumor site by MRI.

Discussion

Pancreatic cancer has one of the worst prognoses among cancers (32). The high malignancy of pancreatic adenocarcinoma prompts the destruction of the surrounding tissue, whereas the lack of serous membrane in healthy pancreas cannot prevent the dissemination of cancer cells. The microenvironment characteristics of the pancreatic adenocarcinoma, including hypovascularity and thick fibrosis, prevent the accumulation of drugs in the tumor tissue (33). Moreover, the anatomic position of the pancreas in the deep retroperitoneal space makes early detection difficult. Although computed tomography is widely used for the evaluation of pancreatic carcinoma in the clinical setting, MRI may better predict the therapeutic efficacy and the prognosis in patients with pancreatic cancer because of its superior contrast resolution of noncontour deforming lesions of the pancreas, small liver metastases, and peritoneal disseminations (34). Thus, the outstanding contrast enhancement achieved by Gd-DTPA/DACHPt–loaded micelles on this tumor model suggests the great potential of this modality for the clear detection of the lesions in the abdominal cavity and the facile recognition of the carcinomas of the pancreas as distinct from the surrounding internal organs by MRI.

The exceptionally bright contrast achieved by Gd-DTPA/DACHPt–loaded micelles can be attributed to the enhanced accumulation of the micelles at the tumor site and to the

augmentation of the relaxivity of the Gd-DTPA in the core of the micelles. The amount of Gd-DTPA delivered by the micelles in the orthotopic pancreatic tumor was >3% of the injected dose after 4 hours. Because the r_1 of Gd-DTPA in the micelles is 24 times higher than that of free Gd-DTPA, the resulting contrast enhancement probably mimics a much higher accumulation level. In this regard, it has been reported that the r_1 of Gd-based MRI contrast agents increases after binding with polymers or proteins due to the flexibility reduction per Gd molecule and the increase of the rotational correlation time (τ_R; ref. 35). Moreover, Livramento and colleagues (36) suggested that an Fe/Gd chelate, a metallostar $Fe\{Gd_2(bipyridine(diethylenetriaminetetraacetic\ acid)_2(H_2O)_4)_3\}^{4-}$ structure, showed a high relaxivity because the inner-sphere water molecules presented an exchange rate (τ_m) close to the optimal value in addition to the increasing τ_R. In our system, the formation of the Gd-DTPA/DACHPt–loaded micelles probably combined an increase of the τ_R and the optimization of the τ_m in the hydrophobic environment at the micelle core, leading to the increase in relaxivity. Further studies are needed to establish the mechanism of the relaxivity enhancement of Gd-DTPA/DACHPt–loaded micelles, and they are currently under way in our laboratory.

The construction of macromolecular MRI contrast agents has been an attractive strategy to achieve diagnostic agents with extended blood circulation. Nevertheless, for Gd-based contrast agents, this approach could increase the risk of toxicity due to the prolonged tissue exposure to those macromolecules and the potential release of Gd^{3+} ions. Thus, the accumulation of high-generation dendrimer contrast agents in the healthy tissues might potentiate the nephrotoxicity and hepatotoxicity risks (37). Accordingly, only 20% of the injected dose of a generation 4–based PAMAM-Gd contrast agent was excreted from the body during the first 2 days, showing transient accumulation in the renal tubules. In contrast to this, the biodistribution of

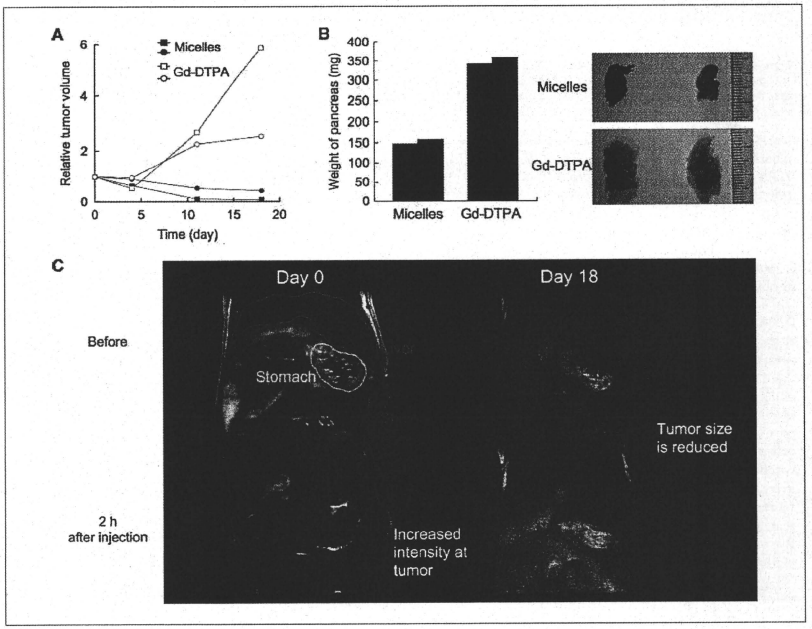

Figure 5. *In vivo* antitumor activity of Gd-DTPA/DACHPt–loaded micelles on orthotopic pancreatic cancer model (BxPC3) assessed by volumetric MRI. A, effect of Gd-DTPA/DACHPt–loaded micelles (8 mg/kg on Pt basis) and Gd-DTPA (30 mg/kg) injected i.v. at day 0, 4, 11 and 18 on the growth of BxPC3 tumors. B, left, weight of the whole pancreas for mice treated with the micelles or Gd-DTPA at day 18 on the antitumor experiment; right, macroscopies of the excised pancreas after treatment with the micelles or Gd-DTPA. C, MRI at days 0 and 18 of a tumor-bearing mouse treated with Gd-DTPA/DACHPt–loaded micelles. The tumor size was 89 mm^3 at day 0 and 5 mm^3 at day 18.

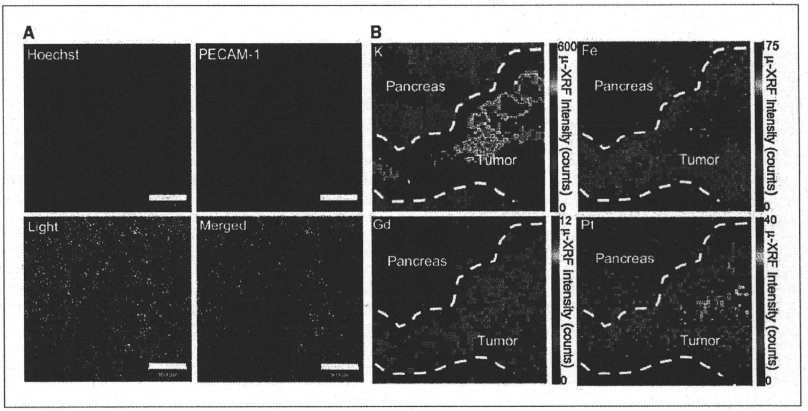

Figure 6. Intratumoral distribution of Gd-DTPA/DACHPt–loaded micelles in orthotopic BxPC3 tumors. A, immunofluorescence microscopy of tumor sections 4 h after injection of the micelles. The cell nuclei were stained with Hoechst, and the blood vessels were marked with PECAM-1 antibody. Scale bars, 100 μm. B, K, Fe, Pt, and Gd distribution in a tumor section including normal pancreatic tissue determined by μ-SR-XRF. Scale bars, 100 μm.

Gd-DTPA/DACHPt–loaded micelles revealed minimal accumulation of Gd-DTPA in normal tissues. Moreover, the Gd-DTPA released from the micelles probably is rapidly excreted from the body because of the relatively fast plasma clearance of low–molecular weight Gd-DTPA, thus eliminating the risk of undesired toxicity.

The real-time observation of drug distribution can increase the accuracy of treatment and enable practitioners to obtain feedback on the therapeutic efficacy at an earlier stage, and promptly adjust the treatment strategy. Gd-DTPA/DACHPt–loaded micelles might be helpful for directly assessing the distribution of the anticancer drugs at early stages by MRI. In this study, the μ-XRF results showed that the delivered Gd-DTPA and DACHPt were colocalized and uniformly distributed within the pancreatic tumors, whereas there was no drug accumulation in healthy pancreas, supporting the strong diagnostic and anticancer effect of the micelles (Fig. 6B, Pt and Gd). Moreover, the chemotherapy regimens are given in periodic cycles, for example, one cycle every 2 weeks during 12 weeks in FOLFOX (folinic acid, fluorouracil, and oxaliplatin) regimen for the treatment of colorectal cancer. By using Gd-DTPA/DACHPt–loaded micelles, the tumor size can be followed up in real-time by imaging at the day of the drug administration. Consequently, the Gd-DTPA/DACHPt–loaded micelles will have significant implications in the design and development of advanced multifunctional nanomedicines with great potential for clinical application as visible DDS.

Disclosure of Potential Conflicts of Interest

No potential conflicts of interest were disclosed.

Acknowledgments

We thank Sayaka Shibata and Teppei Nakahara for their technical assistance on the MRI experiments.

Grant Support

This research was supported by Funding Program for World-Leading Innovative R&D on Science and Technology (FIRST Program) from the Japan Society for the Promotion of Science (JSPS) and Grants-in-Aid for Scientific Research from the Japanese Ministry of Health, Labor, and Welfare (Nanomedicine Project).

The costs of publication of this article were defrayed in part by the payment of page charges. This article must therefore be hereby marked *advertisement* in accordance with 18 U.S.C. Section 1734 solely to indicate this fact.

Received 01/26/2010; revised 06/30/2010; accepted 07/09/2010; published OnlineFirst 08/04/2010.

References

1. Inoue A, Saijo Y, Maemondo M, et al. Severe acute interstitial pneumonia and gefitinib. Lancet 2003;361:137–9.
2. Jones BL. Trastuzumab: hopes and realities. Lancet Oncol 2002;3:137–44.
3. Ewer MS, Vooletich MT, Durand JB, et al. Reversibility of trastuzumab-related cardiotoxicity: new insights based on clinical course and response to medical treatment. J Clin Oncol 2005;23:7820–6.
4. Scappaticci FA, Skillings JR, Holden SN, et al. Arterial thromboembolic events in patients with metastatic carcinoma treated with chemotherapy and bevacizumab. J Natl Cancer Inst 2007;99:1232–9.

5. Davis ME, Chen Z, Shin DM. Nanoparticle therapeutics: an emerging treatment modality for cancer. Nat Rev Drug Discov 2008;7:771–82.
6. Torchilin VP. Recent advances with liposomes as pharmaceutical carriers. Nat Rev Drug Discov 2005;4:145–60.
7. Peer D, Karp JM, Hong S, Farokhzad OC, Margalit R, Langer R. Nanocarriers as an emerging platform for cancer therapy. Nature Nanotech 2007;2:751–60.
8. Ferrari M. Cancer nanotechnology: opportunities and challenges. Nat Rev Cancer 2005;5:161–71.
9. Duncan R. Polymer conjugates as anticancer nanomedicines. Nat Rev Cancer 2006;6:688–701.
10. Kabanov AV, Alakhov VY. Pluronic block copolymers in drug delivery: from micellar nanocontainers to biological response modifiers. Crit Rev Ther Drug Carrier Syst 2002;19:1–73.
11. Nishiyama N, Kataoka K. Current state, achievements, and future prospects of polymeric micelles as nanocarriers for drug and gene delivery. Pharmacol Ther 2006;112:630–48.
12. Matsumura Y, Kataoka K. Preclinical and clinical studies of anticancer agent-incorporating polymer micelles. Cancer Sci 2009;100:572–9.
13. Hashizume H, Baluk P, Morikawa S, et al. Opening between defective endothelial cells explain tumor vessel leakiness. Am J Pathol 2000;156:1363–80.
14. Maeda H. The enhanced permeability and retention (EPR) effect in tumor vasculature: the key role of tumor-selective macromolecular drug targeting. Adv Enzyme Regul 2001;41:189–207.
15. Muggia FM, Hainsworth JD, Jeffers S, et al. Phase II study of liposomal doxorubicin in refractory ovarian cancer: antitumor activity and toxicity modification by liposomal encapsulation. J Clin Oncol 1997;15:987–93.
16. Gradishar WJ, Tjulandin S, Davidson N, et al. Phase III trial of nanoparticle albumin-bound paclitaxel compared with polyethylated castor oil-based paclitaxel in women with breast cancer. J Clin Oncol 2005;23:7794–803.
17. Matsumura Y, Maeda H. A new concept for macromolecular therapeutics in cancer chemotherapy: mechanism of tumoritropic accumulation of proteins and the antitumor agent SMANCS. Cancer Res 1986;46:6387–92.
18. Hamaguchi T, Matsumura Y, Shirao K, et al. Phase I study of novel drug delivery system, NK911, a polymer micelle encapsulated doxorubicin [abstract 571]. Proceedings of the 39th annual meeting of the American Society of Clinical Oncology (ASCO); 2003, May 31-June 3; Chicago, USA.
19. Kato K, Hamaguchi T, Yasui H, et al. Phase I study of NK105, a paclitaxel-incorporating micellar nanoparticle, in patients with advanced cancer. ASCO Annual Meeting Proceedings. J Clin Oncol 2006;24:2018.
20. Burris HA III, Infante JR, Spigel DR, et al. A phase I dose-escalation study of NK012. ASCO Annual Meeting Proceedings. J Clin Oncol 2008;26:2538.
21. Wilson RH, Plummer R, Adam J, et al. Phase I and pharmacokinetic study of NC-6004, a new platinum entity of cisplatin-conjugated polymer forming micelles. J Clin Oncol 2008;26:2573.
22. Dent R, Trudeau M, Pritchard KI, et al. Triple-negative breast cancer: clinical features and patterns of recurrence. Clin Cancer Res 2007;13:4429–34.
23. McCarthy JR, Weissleder R. Multifunctional magnetic nanoparticles for targeted imaging and therapy. Adv Drug Deliv Rev 2008;60:1241–51.
24. McCarthy JR, Jaffer FA, Weissleder R. A macrophage-targeted theranostic nanoparticle for biomedical applications. Small 2006;2:983–7.
25. Pan D, Caruthers SD, Hu G, et al. Ligand-directed nanobialys as theranostic agent for drug delivery and manganese-based magnetic resonance imaging of vascular targets. J Am Chem Soc 2008;130:9186–7.
26. Nasongkla N, Bey E, Ren J, et al. Multifunctional polymeric micelles as cancer-targeted, MRI-ultrasensitive drug delivery systems. Nano Lett 2006;6:2427–30.
27. Weinmann HJ, Brasch RC, Press WR, Wesbey GE. Characteristics of gadolinium-DTPA complex: a potential NMR contrast agent. Am J Roentgenol 1984;142:619–24.
28. Cabral H, Nishiyama N, Okazaki S, Koyama H, Kataoka K. Preparation and biological properties of dichrolo(1,2-diaminocyclohexane) platinum(II) (DACHPt)-loaded polymeric micelles. J Control Release 2005;101:223–32.
29. Gouin S, Winnik F. Quantitative assays of the amount of diethylenetriaminepentaacetic acid conjugated to water-soluble polymers using isothermal titration calorimetry and colorimetry. Bioconjug Chem 2001;12:372–7.
30. Terada Y, Goto S, Takimoto N, et al. Construction and commissioning of BL37XU at SPring-8. AIP Conf Proc 2004;705:376–9.
31. Ventrucci M, Cipolla A, Racchini C, Casadei R, Simoni P, Gullo L. Tumor M2-pyruvate kinase, a new metabolic marker for pancreatic cancer. Dig Dis Sci 2004;49:1149–55.
32. Jemal A, et al. Cancer statistics, 2007. CA Cancer J Clin 2007;57:43–66.
33. Sofuni A, et al. Differential diagnosis of pancreatic tumors using ultrasound contrast imaging. J Gastroenterol 2005;40:518–25.
34. Miller FH, Rini NJ, Keppke AL. MRI of adenocarcinoma of the pancreas. Am J Roentgenol 2006;187:W365–374.
35. Zhang Z, Greenfield MT, Spiller M, McMurry TJ, Lauffer RB, Caravan P. Multilocus binding increases the relaxivity of protein-bound MRI contrast agents. Angew Chem 2005;117:6924–7.
36. Livramento JB, Toth E, Sour A, Borel A, Merbach AE, Ruloff R. High relaxivity confined to a small molecular space: a metallostar-based potential MRI contrast agent. Angew Chem Int Ed 2005;44:1480–4.
37. Duncan R, Izzo L. Dendrimer biocompatibility toxicity. Adv Drug Deliv Rev 2005;57:2215–37.

Cancer Science
The official journal of the Japanese Cancer Association

Hypoglycemic/hypoxic condition *in vitro* mimicking the tumor microenvironment markedly reduced the efficacy of anticancer drugs

Hiroko Onozuka,[1,2] Katsuya Tsuchihara[1] and Hiroyasu Esumi[1,2,3]

[1]Cancer Physiology Project, Research Center for Innovative Oncology, National Cancer Center Hospital East, Kashiwa, Chiba; [2]Department of Integrated Biosciences, Graduate School of Frontier Sciences, The University of Tokyo, Kashiwa, Chiba, Japan

(Received November 23, 2010/Revised January 14, 2011/Accepted January 18, 2011/Accepted manuscript online January 21, 2011/Article first published online March 7, 2011)

Tumor tissues are often hypoxic because of defective vasculature. We previously showed that tumor tissues are also often deprived of glucose. The efficacy of anticancer drugs is affected by the tumor microenvironment, partly because of the drug delivery and cellular drug resistance; however, the precise mechanisms remain to be clarified. In the present study, we attempted to clarify whether hypoglycemic/hypoxic condition, which mimics the tumor microenvironment, might induce drug resistance, and if it did, to elucidate the underlying mechanisms. Pancreatic cancer-derived PANC-1 cells were treated with serial dilutions of anticancer drugs and incubated in either normoglycemic (1.0 g/L glucose) or hypoglycemic (0 g/L glucose) and normoxic (21% O_2) or hypoxic (1% O_2) conditions. The 50% inhibitory concentration of gemcitabine was 1000 times higher for PANC-1 cells incubated under the hypoglycemic/hypoxic condition than for those incubated under the normoglycemic/normoxic condition. Conventional anticancer drugs target rapidly growing cells, so that non-proliferating or slowly proliferating cells usually show resistance to drugs. Though the cell cycle was delayed, sufficient cellular uptake and DNA incorporation of gemcitabine occurred under the hypoglycemic/hypoxic condition to cause DNA lesions and S-phase arrest. To overcome hypoglycemic/hypoxia-induced drug resistance, we examined kinase inhibitors targeting Chk1 or cell-survival signaling pathways. Among the compounds examined, the combination of UCN-01 and LY294002 partially sensitized the cells to gemcitabine under the hypoglycemic/hypoxic condition. These findings suggested that the adoption of suitable strategies may enhance the cytotoxicities of clinically used anticancer drugs against cancer cells. (*Cancer Sci* 2011; 102: 975–982)

It is widely accepted that solid tumors are heterogeneous in structure as a result of unregulated cancer cell proliferation, presence of several cell types and aberrant vessel formation. Among these, the tumor vasculature has a major impact on the tumor microenvironment. In normal tissue, vascular networks generally develop in a well-ordered hierarchal fashion, so that an insufficient blood supply seldom occurs. In contrast, tumor vascular networks undergo continuous remodeling, because unregulated cell proliferation destroys the existing tissue structures. Previous structural analyses had clearly shown that tumors exhibit aberrant and poorly organized vasculature without any hierarchy.[1–4]

As a consequence of the poorly organized vasculature in tumors, the delivery of oxygen is extremely limited. Direct measurement of the oxygen tension in cancer tissues has demonstrated the presence of severely hypoxic regions in many types of cancers.[5] Although hypoxia is also toxic to cancer cells, cancer cells adapt through genetic and epigenetic changes that allow them to survive and even proliferate in hypoxic environments.[6–9] Hypoxia-inducible factor-1α (HIF-1α) is a key transcription factor for downstream hypoxia-inducible genes, which regulate several biological processes in hypoxic environments.[10–12] Hypoxia response pathways overlap with many of the known oncogenic signaling pathways and also contribute to tumor aggressiveness.[13–15] Therefore, tumor hypoxia is regarded as a good target for cancer therapy. Meanwhile, cancer cells predominantly use the glycolytic pathway, rather than oxidative phosphorylation, for energy production, irrespective of the oxygen availability (Warburg effect).[16,17] In addition to the intrinsic predisposition of cancer cells to metabolize glucose, HIF-1α has been shown to regulate the expressions of all the enzymes involved in the glycolytic pathway, which mediate cellular glucose uptake.[18,19] The activation of HIF-1α enables cancer cells to use excessive glucose to maintain cellular homeostasis in hypoxic environments, causing depletion of glucose from the surrounding tissues. Indeed, a metabolomic analysis of stomach and colon cancer tissues has clearly showed glucose depletion in the tumor tissues as compared to normal tissues, indicating that several regions of tumor tissues are characterized by both hypoxia and hypoglycemia.[20] However, little is known about the biology of cancer cells under hypoglycemic condition.

Although many molecular-targeting drugs have been introduced for clinical use, conventional anticancer drugs are in wide clinical use and continue to confer many clinical benefits. Heterogeneity in the tumor microenvironment provides cancer cells the opportunity to escape from anticancer drugs. One of the processes affected by the heterogeneity of tumors is drug diffusion.[21,22] In addition, many types of drug resistance of the cells to anticancer drugs are known to occur, and overexpression of the ABC transporter is a representative mechanism.[23–25] Recent studies have reported that drug resistance may also be related to the tumor microenvironment, especially hypoxia, and the clinical relevance of such resistance. Three-dimensional culture system is used as a useful new strategy to represent tumor microenvironment *in vitro*.[26,27] However, the detailed molecular mechanisms for the resistance are largely unclear. In this study, we clarified how hypoglycemic/hypoxic condition might affect the efficacies of anticancer drugs.

Materials and Methods

Cell lines and culture conditions. The human pancreatic ductal adenocarcinoma cell lines PANC-1 and Capan-1 and the hepatoma-derived cell line HepG2 were purchased from ATCC (American Type Culture Collection, Rockville, MD, USA). PSN-1 was gifted from the Genetics Division of the National Cancer Center Research Institute (Tokyo, Japan). All cell lines were maintained in DMEM (Nissui, Tokyo, Japan). A

[3]To whom correspondence should be addressed. E-mail: hesumi@east.ncc.go.jp

doi: 10.1111/j.1349-7006.2011.01880.x

glucose-deprived condition was achieved by culturing the cells in glucose-free medium (Sigma, St. Louis, MO, USA). A hypoxic condition was achieved by incubating the cells in a hypoxia incubator in the presence 5% CO_2 and 1% O_2. The experiments were performed using PANC-1 cells, unless stated otherwise.

Reagents. Gemcitabine (Gemzar; Eli Lilly Co., Indianapolis, IN, USA) and 5-fluorouracil (Kyowa Hakko Kirin Co., Ltd, Tokyo, Japan) were dissolved in saline and stored at −20°C. Cisplatin (Sigma) was dissolved in DMSO on the day of use. UCN-01 was kindly provided by Kyowa Hakko Kirin Co., Ltd. LY294002 and Gö6976 were purchased from Calbiochem (San Diego, CA, USA). Antibodies were purchased from the following manufacturers: anti-total Akt, anti-phosphospecific Akt (Ser 473), anti-phosphospecific Cdc25c (Ser216), anti-phosphor specific Chk1 (Ser345), anti-phosphospecific Chk2 (Thr68), and anti-γ-H2AX (Ser139) from Cell Signaling Technology (Danvers, MA, USA); anti-HIF-1α and anti-HIF-2α antibodies from Novus Biologicals (Littleton, CO, USA); Chk1 (G-4) and Actin (C-11) antibodies from Santa Cruz Biotechnology (Santa Cruz, CA, USA); Chk2 antibody clone7 from Upstate Biotechnology (Lake Placid, NY, USA). The following secondary antibodies were purchased from Santa Cruz Biotechnology: goat antimouse IgG-HRP, goat antirabbit IgG-HRP, and donkey antigoat IgG-HRP.

Cytotoxicity assay of anticancer drugs. The cytotoxicity assay was performed using Cell Counting kit-8 (Dojindo Molecular Technologies, Kumamoto, Japan), as described previously.[28] The cell number in the absence of anticancer drugs under each culture condition was set as 100%. Values shown represent the means ± SD (n = 4–8).

siRNA transfection. SMARTpool HIF-1α, HIF-2α, Chk1, Chk2 and non-silencing siRNA were purchased from Dharmacon (Lafayette, CO, USA). Cells were seeded at 10^6 cells per dish in 10 mm dishes. At 24 h after seeding, siRNA was added at a final concentration of 100 nM, followed by incubation for 24 h. The knockdown efficacies were determined by Western blot analysis.

Western blot analysis. Protein extraction and Western blot analysis were performed as described previously.[29] The antibody dilutions used were in accordance with the manufacturers' instructions.

Cell cycle analysis. After 24 h preincubation, 1×10^6 cells were cultured in a 60-mm cell culture dish under either normoglycemic/normoxic or hypoglycemic/hypoxic conditions for 24 h, followed by staining using the Click-iT EdU Alexa Fluor 488 Cell Proliferation Assay kit (Molecular Probes, Eugene, OR, USA) in accordance with the manufacturer's instructions, and analyzed on a FACSCalibur (BD Bioscience, San Jose, CA, USA).

DNA ploidy assay. After 24 h preincubation, 1×10^6 cells were cultured in a 60-mm cell culture dish under either normoglycemic/normoxic or hypoglycemic/hypoxic conditions in the presence or absence of 1 μM gemcitabine for 24 h, followed by staining with propidium iodide (Molecular Probes) in accordance with the manufacturer's instruction, and analyzed on a FACSCalibur.

[^{3}H]-Gemcitabine and [^{3}H]-thymidine uptake. After 24 h preincubation, 1×10^6 cells were cultured in a 60-mm cell culture dish under either normoglycemic/normoxic or hypoglycemic/hypoxic conditions for 24 h, followed by incubation for another 3 h with 1 μM [^{3}H]-labeled gemcitabine (6.8 μCi/nmol; Moravek Biochemicals, Brea, CA, USA). The cells were washed thrice with complete medium containing 100 μM gemcitabine, and twice with ice-cold PBS. The cells were detached by trypsinization and counted by the Trypan blue exclusion method. The total cellular uptake of [^{3}H]-gemcitabine was measured by lysing a 10 μL aliquot of the cell suspension and counting the total cell-associated radioactivity using a multipurpose scintillation counter, LS6500 (Beckman Coulter Inc., Fullerton, CA, USA). The incorporation of [^{3}H]-gemcitabine into the DNA was determined by a previously published method, with slight modification.[30]

Statistical analysis. All the results were expressed as the mean ± SD. The statistical analysis was conducted using the Student t-test after an ANOVA.

Results

Effect of the culture condition on the sensitivity to various anticancer drugs. In the first set of experiments, we determined whether hypoxia and hypoglycemia might affect the sensitivity of the cancer cells to gemcitabine, 5-fluorouracil and cisplatin, which are commonly used drugs for systemic chemotherapy of cancer. Pancreatic cancer-derived PANC-1 cells were treated with serial dilutions of anticancer drugs and incubated under either a normoglycemic (1.0 g/L glucose) or hypoglycemic (0 g/L glucose) condition and normoxic (21% O_2) or hypoxic (1% O_2) condition. The 50% inhibitory concentration (IC_{50}) of gemcitabine for the PANC-1 cells incubated under the normoglycemic/normoxic condition was 300 nM, whereas the IC_{50} values of gemcitabine under the hypoxic and hypoglycemic condition were >300 μM, which was 1000 times higher than the value under the normoglycemic/normoxic condition (Fig. 1A). Similarly, the IC_{50} of 5-fluorouracil was greatly influenced by the culture condition, with IC_{50} values of 2.7 μM under the normoglycemic/normoxic condition, 9.6 μM under the hypoglycemic/normoxic condition, 92 μM under the normoglycemic/hypoxic condition, and 79 μM under the hypoglycemic/hypoxic condition (Fig. 1B); the corresponding values for cisplatin were 74, 106, 108 μM, and more than 300 μM (Fig. 1C). The cytotoxicities of gemcitabine for other pancreatic cancer cell lines, PSN-1 and Capan-1, were also examined. The IC_{50} of gemcitabine for the PSN-1 cells was 0.22 μM under the normoglycemic/normoxic condition and more than 300 μM under the hypoglycemic/hypoxic condition (Fig. 1D). The IC_{50} of gemcitabine for the Capan-1 cells was 0.24 μM under the normoglycemic/normoxic condition, and 57 μM under the hypoglycemic/hypoxic condition (Fig. 1E). The sensitivities of the hepatoma-derived HepG2 cells, which express wild-type p53, were also examined. The IC_{50} of gemcitabine for HepG2 cells was 2.9 μM under the normoglycemic/normoxic condition, and more than 300 μM under the hypoglycemic/hypoxic condition (Fig. 1F).

Cell-cycle progression and gemcitabine uptake under various culture conditions. During cell proliferation, cells must prepare to double all their components. The restriction of nutrient and oxygen supply might greatly influence the cell-cycle progression, through complex mechanisms.[31] Gemcitabine is incorporated into the DNA to exert its cytotoxicity.[32,33] Therefore, the cell-cycle analysis was conducted under the hypoglycemic/hypoxic condition. Newly synthesized DNA was labeled with 5-ethynil-2′-deoxyuridine (EdU), and the DNA content was labeled with 7-aminoactinomycin D, followed by multicolor analysis by flow-cytometry. About 45% of the cells under the normoglycemic/normoxic condition and 41% of the cells under the hypoglycemic/hypoxic condition were in the S-phase. Thus, the S-phase population was almost the same under both conditions. Closer analysis of the S-phase populations under both conditions indicated that the numbers of cells in the late S and G2 phases were reduced under the hypoglycemic/hypoxic condition, indicating S-phase prolongation (Fig. 2A). The cellular uptake and DNA incorporation of gemcitabine were directly assessed using [^{3}H]-labeled gemcitabine. Cells were cultured under the normoglycemic/normoxic or hypoglycemic/hypoxic condition for 24 h, followed by incubation with 1 μM [^{3}H]-gemcitabine for 3 h. The cellular uptake of gemcitabine was almost

doi: 10.1111/j.1349-7006.2011.01880.x

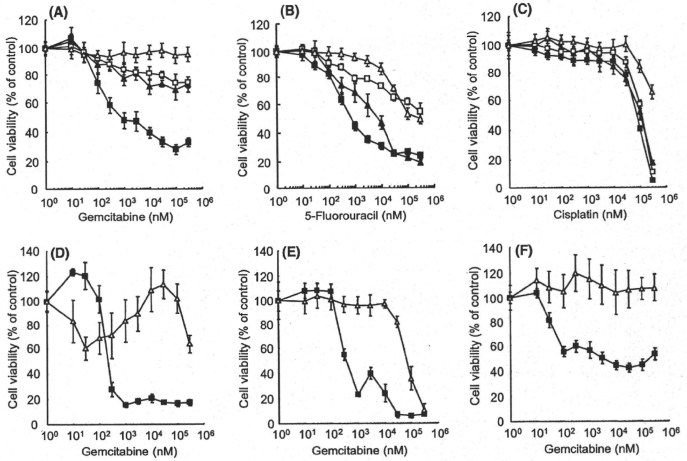

Fig. 1. Effect of the culture condition on the cytotoxicity of anticancer drugs. The cytotoxicity of (A) gemcitabine, (B) 5-fluorouracil and (C) cisplatin on the PANC-1 cells was examined. Cytotoxicity of gemcitabine on (D) the Capan-1, (E) PSN-1 and (F) HepG2 cells were also examined. (■) normoglycemic/normoxic, (▲) hypoglycemic/normoxic, (□) normoglycemic/hypoxic, and (△) hypoglycemic/hypoxic conditions.

twofold higher and the DNA incorporation of [^{3}H]-gemcitabine was almost fivefold higher under the hypoglycemic/hypoxic condition than under the normoglycemic/normoxic condition (Fig. 2B).

Gemcitabine-induced checkpoint activation and S-phase arrest. DNA incorporation of gemcitabine cause the replication fork to stall; this, in turn, induces S-phase checkpoint activation and S-phase arrest or apoptosis.[34,35] To analyze the signaling by gemcitabine-induced DNA lesions, we examined checkpoint kinase activations. After 12 h incubation in the presence or absence of 1 and 100 μM gemcitabine, phosphorylation of H2AX, Chk1 and Chk2 were induced by gemcitabine equally under different culture conditions (Fig. 2C). We further examined gemcitabine-induced S-phase arrest using propidium iodide staining and flow-cytometric analysis. S-phase arrest was equally induced by gemcitabine under the normoglycemic/normoxic and hypoglycemic/hypoxic conditions (Fig. 2D).

Effect of inhibition of Chk1 signaling on the cytotoxicity of gemcitabine. Previous studies have shown that UCN-01 and Gö6976 sensitized cells to gemcitabine via Chk1 inhibition, resulting in abrogation of the cell cycle arrest and subsequent cell death.[36–39] We examined the sensitivity of Chk1 signaling-inhibited cells to gemcitabine under the hypoglycemic/hypoxic condition. Western blot analysis showed that 1 μM of the Chk1 inhibitors, UCN-01 and Gö6976, reduced the phosphorylation of cdc25c, a downstream mediator of Chk1 (Fig. 3A); UCN-01 and Gö6976 lowered the IC_{50} of gemcitabine by more than 10 times under the normoglycemic/normoxic condition, but not under the hypoglycemic/hypoxic condition (Fig. 3B,C). Similar results were obtained with 10 μM UCN-01 or Gö6976. To confirm these results, the effect of an RNAi for Chk1 was examined. The RNAi effectively suppressed Chk1 activation under both the normoglycemic/normoxic and hypoglycemic/hypoxic conditions (Fig. 3D); however, Chk1 suppression enhanced the sensitivity of the cells to gemcitabine only under the normoglycemic/normoxic condition (Fig. 3E).

Effect of inhibition of the HIFs and PI3K/Akt signaling on the sensitivity of the cancer cells to gemcitabine. HIF-1α is induced by hypoxia and modifies cell survival.[40,41] Under the hypoxic condition, the HIF-1α protein levels increased rapidly to peak within 2 h and thereafter decreased (Fig. 4A). The HIF-2α protein level was also rapidly induced within 2 h, and maintained for 24 h. The HIF-1α protein level decreased, but not the HIF-2α protein levels, under the hypoglycemic condition (Fig. 4A). To evaluate the involvement of the HIFs in the resistance to gemcitabine, HIF-1α or HIF-2α expression was suppressed by RNAi and the sensitivity of the cells to gemcitabine was examined. RNAi for HIF-1α and HIF-2α effectively suppressed the hypoxia-induced accumulation of the respective proteins (Fig. 4B). Knockdown of HIF-1α, HIF-2α or HIF-1/2α did not have any effect on the sensitivity of the cells to gemcitabine under hypoxic condition (Fig. 4C–E). Akt is known to be activated by hypoglycemic condition and to play some roles in cell survival.[42,43] In our study, marked increase of Akt phosphorylation at ser473 was observed within 2 h under both the hypoglycemic and hypoxic condition, which was sustained for at least 24 h; the increase was, however, more evident under the hypoxic condition (Fig. 4A). To examine the involvement of PI3K/Akt signaling in the drug resistance, we utilized a PI3K inhibitor, LY294002. After treatment with LY294002 (10 and 20 μM) for 24 h, Akt phosphorylation was effectively inhibited to less than the basal level (Fig. 4F). Although treatment with 20 μM of LY294002 reduced the IC_{50} of gemcitabine by 15-fold under the normoglycemic/normoxic condition, it had little effect under the hypoglycemic/normoxic condition (Fig. 4G).

Effect of combined inhibition of Chk1 and HIF signaling on the drug resistance induced by hypoglycemic/hypoxic condition. Inhibition of either checkpoint to produce release from the gemcitabine-induced S-phase arrest or of cell-survival signaling under hypoxia, HIFs, and under hypoglycemia Akt, each alone was not effective to ameliorate the resistance to gemcitabine. We examined the combined inhibition of Chk1 and

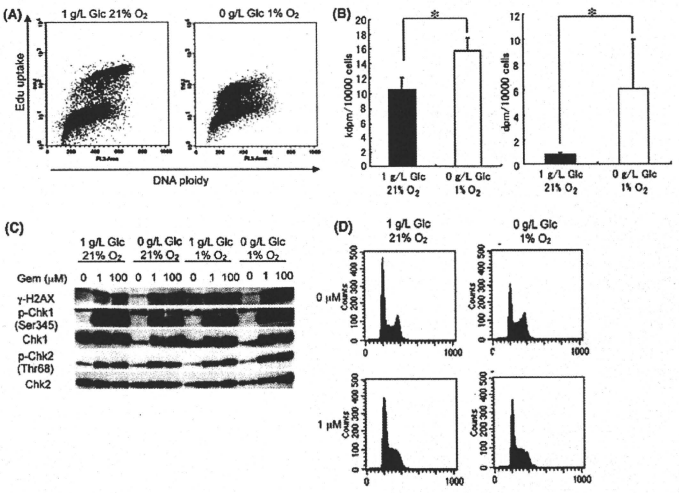

Fig. 2. Cell-cycle progression, uptake of gemcitabine and gemcitabine-induced cellular responses under various conditions. (A) Representative cell-cycle distribution detected by EdU incorporation and flow cytometry. Three independent experiments were carried out. (B) Cellular uptake and DNA incorporation of [^{3}H] gemcitabine (*$P < 0.05$). (C) Phosphorylations of H2AX, Chk1 and Chk2 detected by Western blot analysis after 12 h treatment with the indicated concentration of gemcitabine. (D) Representative DNA ploidy patterns after 24 h treatment with 1 μM gemcitabine. Three independent experiments were carried out.

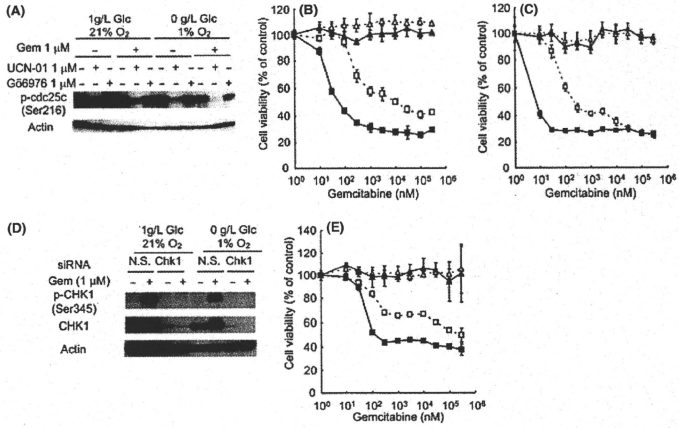

Fig. 3. Effect of inhibition of Chk1 signaling on the sensitivity of cells to gemcitabine. (A) Western blot analysis of cdc25c in the presence of Chk1 inhibitors under the indicated conditions. Cytotoxicity of gemcitabine in the presence or absence of 1 μM (B) UCN-01, (C) or Gö6976 under (■ or □) normoglycemic/normoxic condition or (▲ or △) hypoglycemic/normoxic condition. (D) Western blot analysis of Chk1 expression and activation. (E) The cytotoxicity of gemcitabine with or without Chk1 knockdown under (□ or ■) normoglycemic/normoxic condition or (△ or ▲) hypoglycemic/hypoxic condition.

doi: 10.1111/j.1349-7006.2011.01880.x

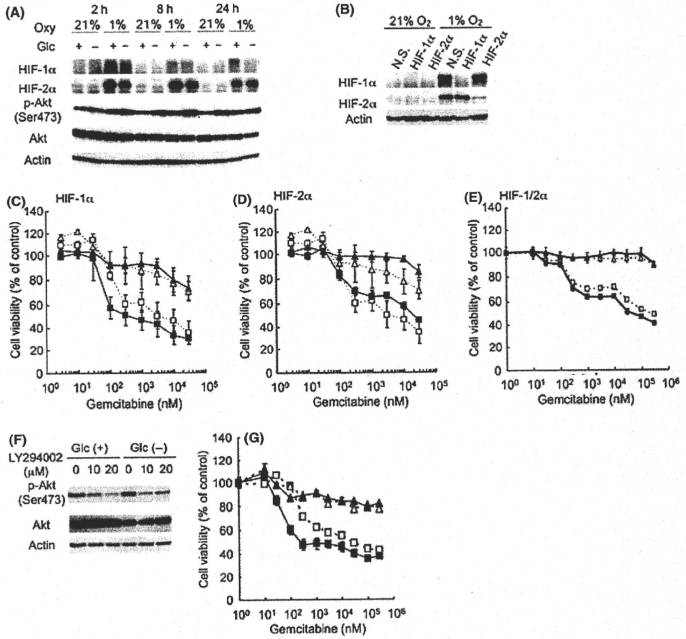

Fig. 4. Effects of inhibition of HIFs and PI3K/Akt signaling on the sensitivity of the cells to gemcitabine. (A) Western blot analysis for HIF1α and 2α accumulation and Akt phosphorylation under the indicated oxygen tension, normoxia (21%), or hypoxia (1%), and in the presence of a glucose concentration of 1 g/L (+) or 0 g/L (−). (B) Western blot analysis for HIF1α and 2α protein in cells treated with HIF-1α or HIF-2α siRNA. The cytotoxicity of gemcitabine on (C) HIF-1α, (D) HIF-2α or (E) HIF-1/2α knockdown cells or control cells under (■ or □) normoglycemic/normoxic condition or (▲ or △) normoglycemic/hypoxic condition. (F) Phosphorylation of Akt in the presence of 10 or 20 μM LY294002 under the indicated culture conditions. (G) Cytotoxicity of gemcitabine in the presence or absence of 20 μM LY294002 under (■ or □) normoglycemic/normoxic condition or (▲ or △) hypoglycemic/normoxic condition.

HIF signaling: HIF-1α, HIF-2α, or HIF-1/2α knockdown cells were examined for their sensitivity to gemcitabine in the presence of 1 μM UCN-01; however, even such combined inhibition was found to have no effect on the sensitivity of the cells to gemcitabine under the hypoxic condition (Fig. 5).

Effect of combined inhibition of Chk1 and PI3K signaling on the drug resistance induced by hypoglycemic/hypoxic condition. Combined inhibition of Chk1 and PI3K signaling was examined. As shown in Figure 6 1μM UCN-01 and 20 μM LY294002 strongly enhanced gemcitabine cytotoxicity under both normoglycemic/normoxic and hypoglycemic/hypoxic conditions, although the effect under the hypoglycemic/hypoxic condition was less pronounced (Fig. 6A). On the other hand, combined treatment with 1 μM Gö6976 and 20 μM LY294002 enhanced the sensitivity of the cells to gemcitabine only under the normoglycemic/normoxic condition (Fig. 6B). In order to confirm if the effect of UCN-01 was due to inhibition of Chk1 activation or inhibition of some other target, the effect of the RNAi on Chk1 activation was examined. Chk1 siRNA and 20 μM LY294002 enhanced the sensitivity of the cells to gemcitabine under the normoglycemic/normoxic condition; however, it had no any effect under the hypoglycemic/hypoxic condition.

Discussion

As clearly shown in the present work, hypoxia and hypoglycemia had a large impact on the cellular sensitivity to anticancer drugs in different cancer cell lines. In most cases, the mechanism underlying the drug resistance is regarded as decreased cellular drug uptake. Multidrug resistance is one of major cellular mechanisms of drug resistance to a broad spectrum of anticancer drugs, and this phenotype is associated with an increased drug efflux from the cells caused by overexpression of the ABC transporter. In the present work, hypoglycemic/hypoxic condition also induced multidrug resistance; however, our findings clearly indicated that there was no reduction of gemcitabine uptake and incorporation under the hypoglycemic/hypoxic condition. The S-phase population was similar under the normoglycemic/normoxic and hypoglycemic/hypoxic conditions, with accompanying S-phase prolongation. S-phase prolongation might be due to the depletion of *de novo* synthesis of nucleotides caused by

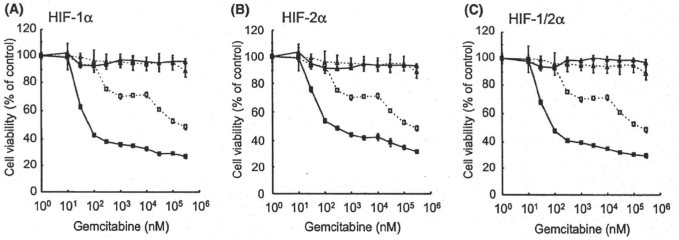

Fig. 5. Effect of combined inhibition of Chk1 and HIF signaling on the sensitivity of the cells to gemcitabine. Cells were treated with gemcitabine in the presence or absence of 1 μM UCN-01 plus RNAi for (A) HIF-1α, (B) HIF-2α or (C) HIF-1/2α under (■ or □) normoglycemic/normoxic condition or (▲ or △) normoglycemic/hypoxic condition.

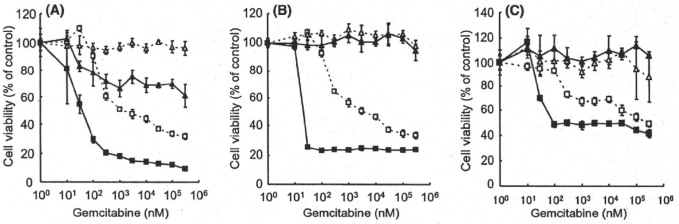

Fig. 6. Effect of combined inhibition of Chk1 and PI3K on the sensitivity of the cells to gemcitabine. Cells were treated with gemcitabine in the presence or absence of 1 μM (A) UCN-01, (B) 1 μM Gö6976 or (C) RNAi for Chk1, and 20 μM LY294002 under (■ or □) normoglycemic/normoxic condition or (▲ or △) hypoglycemic/hypoxic condition.

insufficiency of the pentose phosphate shunt supply. Nevertheless, it was not involved in DNA incorporation of gemcitabine under the hypoglycemic/hypoxic condition. Following its incorporation into DNA, gemcitabine blocks the extension of DNA and stall replication forks, leading to DNA damage. The DNA damage is recognized by sensor molecules that recruit and phosphorylate H2AX protein in the damaged DNA region.[44] Sensor molecules also phosphorylate checkpoint kinase causing its activation and arresting the cell cycle in the S phase.[45] The present study showed that phosphorylation of H2AX, Chk1 and Chk2 were induced by gemcitabine equally under the normoglycemic/normoxic and hypoglycemic/hypoxic conditions, leading to S-phase arrest. During checkpoint kinase activation and cell cycle arrest, phosphorylation of H2AX is known to be recruited by other DNA repair proteins, such as Mre11/Rad50/Nbs1, in the DNA damage region, resulting in activation of the DNA repair pathway.[46,47] Chronic hypoxia has been reported to suppress DNA repair protein activity.[48,49] The increased DNA incorporation of gemcitabine under the hypoglycemic/hypoxic condition may be caused by suppression of the DNA repair pathway.

Modulation of the cellular responses to DNA-damaging agents by checkpoint abrogators or inhibitors of cell survival signaling is an active area of research, since it has been believed that the interference of these signalings may enhance the therapeutic efficacy of anticancer drugs.[50] The S-phase checkpoint consists of a hierarchal regulatory cascade initiated by the activation of Chk1. In the present work, Chk1 inhibitors and Chk1 siRNA enhanced the cytotoxicity of gemcitabine under the normoglycemic/normoxic condition, consistent with other reports.[51–54] However, the abrogation of Chk1 activation did not affect the sensitivity of the cells to gemcitabine under the hypoglycemic/hypoxic condition. Tumor hypoxia has been well-studied, and previous reports have proposed that HIF-1α plays a critical role in determining cell survival and death,[40,41] while knockdown of HIF1α or HIF2α using siRNA did not affect the sensitivity of the cells to gemcitabine under the hypoxic condition in the present study. The PI3K/Akt pathway is well-known for its anti-apoptotic and cell survival activity under various conditions, including hypoxia and hypoglycemia,[55–57] but our results showed that the PI3K inhibitor LY294002 sensitized the cells to gemcitabine only under the normoglycemic/normoxic condition. We examined combined inhibition of Chk1 and of the cell survival pathways-sensitized cells to gemcitabine under the hypoglycemic/hypoxic condition. In the present work, the combination of UCN-01 and LY294002 partly abrogated the hypoglycemic/hypoxia-induced drug resistance, whereas the combination of Gö6976 or Chk1 siRNA with LY294002 had no such effect. These observations suggest that UCN-01 had a different target from Gö6976 in the mechanism of sensitizing the cells to gemcitabine under the hypoglycemic/hypoxic condition. UCN-01 has been reported to induce apoptosis in S-phase-arrested cells, not through Chk1 inhibition, although the precise mechanisms remain poorly understood.[58] We attempted to identify the kinase signaling responsible for the hypoglycemic/hypoxia-induced drug resistance in the targets of UCN-01; however, we did not obtain any clear results. PI3K and Akt are strongly expressed in some cancers, and have been found to be associated with a poor prognosis and increased tumor aggressiveness.[59,60] We previously reported that Akt

doi: 10.1111/j.1349-7006.2011.01880.x

expression was closely associated with cellular tolerance for nutrient deprivation.[61] The present work showed that Akt phosphorylation had a significant impact on the sensitivity of the PANC-1 cells to anticancer drugs.

In this study, we showed that hypoglycemic/hypoxic condition induced multidrug resistance. Combined kinase activations were involved in the hypoglycemic/hypoxia-induced drug resistance. Although the mechanism of cell death caused by gemcitabine is still unclear, the combined strategies described in the text might enhance the cytotoxicity of gemcitabine in clinical practice.

Acknowledgments

This work was supported by a Grant for the Third-Term Comprehensive 10-year Strategy for Cancer Control and 5-year Strategy for the Creation of Innovative Pharmaceuticals and Medical Devices from the Ministry of Health, Labour and Welfare, Japan.

Disclosure statement

No conflict of interest.

References

1 Jain RK. Molecular regulation of vessel maturation. *Nat Med* 2003; **9**: 685–93.
2 Thomlinson RH, Gray LH. The histological structure of some human lung cancers and the possible implications for radiotherapy. *Br J Cancer* 1955; **9**: 539–49.
3 Less JR, Skalak TC, Sevick EM, Jain RK. Microvascular architecture in a mammary carcinoma: branching patterns and vessel dimensions. *Cancer Res* 1991; **51**: 265–73.
4 Brown JM, Giaccia AJ. The unique physiology of solid tumors: opportunities (and problems) for cancer therapy. *Cancer Res* 1998; **58**: 1408–16.
5 Hockel M, Vaupel P. Tumor hypoxia: definitions and current clinical, biologic, and molecular aspects. *J Natl Cancer Inst* 2001; **93**: 266–76.
6 Harris AL. Hypoxia – a key regulatory factor in tumour growth. *Nat Rev Cancer* 2002; **2**: 38–47.
7 Bertout JA, Patel SA, Simon MC. The impact of O_2 availability on human cancer. *Nat Rev Cancer* 2008; **8**: 967–75.
8 Gatenby RA, Gillies RJ. Why do cancers have high aerobic glycolysis? *Nat Rev Cancer* 2004; **4**: 891–9.
9 Gillies RJ, Raghunand N, Karczmar GS, Bhujwalla ZM. MRI of the tumor microenvironment. *J Magn Reson Imaging* 2002; **16**: 430–50.
10 Semenza GL. HIF-1, O(2), and the 3 PHDs: how animal cells signal hypoxia to the nucleus. *Cell* 2001; **107**: 1–3.
11 Price BD, Calderwood SK. Gadd45 and Gadd153 messenger RNA levels are increased during hypoxia and after exposure of cells to agents which elevate the levels of the glucose-regulated proteins. *Cancer Res* 1992; **52**: 3814–7.
12 Wang GL, Semenza GL. Characterization of hypoxia-inducible factor 1 and regulation of DNA binding activity by hypoxia. *J Biol Chem* 1993; **268**: 21513–8.
13 Ryan HE, Lo J, Johnson RS. HIF-1 alpha is required for solid tumor formation and embryonic vascularization. *The EMBO J* 1998; **17**: 3005–15.
14 Maxwell PH, Dachs GU, Gleadle JM *et al.* Hypoxia-inducible factor-1 modulates gene expression in solid tumors and influences both angiogenesis and tumor growth. *Proc Natl Acad Sci U S A* 1997; **94**: 8104–9.
15 Carmeliet P, Dor Y, Herbert JM *et al.* Role of HIF-1alpha in hypoxia-mediated apoptosis, cell proliferation and tumour angiogenesis. *Nature* 1998; **394**: 485–90.
16 Warburg O. On the origin of cancer cells. *Science* 1956; **123**: 309–14.
17 Vander Heiden MG, Cantley LC, Thompson CB. Understanding the Warburg effect: the metabolic requirements of cell proliferation. *Science* 2009; **324**: 1029–33.
18 Chen Z, Lu W, Garcia-Prieto C, Huang P. The Warburg effect and its cancer therapeutic implications. *J Bioenerg Biomembr* 2007; **39**: 267–74.
19 Kondoh H. Cellular life span and the Warburg effect. *Exp Cell Res* 2008; **314**: 1923–8.
20 Hirayama A, Kami K, Sugimoto M *et al.* Quantitative metabolome profiling of colon and stomach cancer microenvironment by capillary electrophoresis time-of-flight mass spectrometry. *Cancer Res* 2009; **69**: 4918–25.
21 Savage P, Stebbing J, Bower M, Crook T. Why does cytotoxic chemotherapy cure only some cancers? *Nat Clin Pract Oncol* 2009; **6**: 43–52.
22 Minchinton AI, Tannock IF. Drug penetration in solid tumours. *Nat Rev Cancer* 2006; **6**: 583–92.
23 Tsuruo T, Naito M, Tomida A *et al.* Molecular targeting therapy of cancer: drug resistance, apoptosis and survival signal. *Cancer Sci* 2003; **94**: 15–21.
24 Sugimoto Y, Tsuruo T. DNA-mediated transfer and cloning of a human multidrug-resistant gene of adriamycin-resistant myelogenous leukemia K562. *Cancer Res* 1987; **47**: 2620–5.
25 Hamada H, Tsuruo T. Functional role for the 170- to 180-kDa glycoprotein specific to drug-resistant tumor cells as revealed by monoclonal antibodies. *Proc Natl Acad Sci U S A* 1986; **83**: 7785–9.
26 Ho WJ, Pham EA, Kim JW *et al.* Incorporation of multicellular spheroids into 3-D polymeric scaffolds provides an improved tumor model for screening anticancer drugs. *Cancer Sci* 2010; **101**: 2637–43.
27 Liao Q, Hu Y, Zhao YP, Zhou T, Zhang Q. Assessment of pancreatic carcinoma cell chemosensitivity using a three-dimensional culture system. *Chin Med J (Engl)* 2010; **123**: 1871–7.
28 Lu J, Kunimoto S, Yamazaki Y, Kaminishi M, Esumi H. Kigamicin D, a novel anticancer agent based on a new anti-austerity strategy targeting cancer cells' tolerance to nutrient starvation. *Cancer Sci* 2004; **95**: 547–52.
29 Awale S, Lu J, Kalauni SK *et al.* Identification of arctigenin as an antitumor agent having the ability to eliminate the tolerance of cancer cells to nutrient starvation. *Cancer Res* 2006; **66**: 1751–7.
30 Wong SJ, Myette MS, Wereley JP, Chitambar CR. Increased sensitivity of hydroxyurea-resistant leukemic cells to gemcitabine. *Clin Cancer Res* 1999; **5**: 439–43.
31 Imamura T, Kanai F, Kawakami T *et al.* Proteomic analysis of the TGF-beta signaling pathway in pancreatic carcinoma cells using stable RNA interference to silence Smad4 expression. *Biochem Biophys Res Commun* 2004; **318**: 289–96.
32 Sampath D, Rao VA, Plunkett W. Mechanisms of apoptosis induction by nucleoside analogs. *Oncogene* 2003; **22**: 9063–74.
33 Ewald B, Sampath D, Plunkett W. Nucleoside analogs: molecular mechanisms signaling cell death. *Oncogene* 2008; **27**: 6522–37.
34 Zhang YW, Hunter T, Abraham RT. Turning the replication checkpoint on and off. *Cell Cycle* 2006; **5**: 125–8.
35 Sampath D, Shi Z, Plunkett W. Inhibition of cyclin-dependent kinase 2 by the Chk1-Cdc25A pathway during the S-phase checkpoint activated by fludarabine: dysregulation by 7-hydroxystaurosporine. *Mol Pharmacol* 2002; **62**: 680–8.
36 Facchinetti MM, De Siervi A, Toskos D, Senderowicz AM. UCN-01-induced cell cycle arrest requires the transcriptional induction of p21(waf1/cip1) by activation of mitogen-activated protein/extracellular signal-regulated kinase kinase/extracellular signal-regulated kinase pathway. *Cancer Res* 2004; **64**: 3629–37.
37 Monks A, Harris ED, Vaigro-Wolff A, Hose CD, Connelly JW, Sausville EA. UCN-01 enhances the in vitro toxicity of clinical agents in human tumor cell lines. *Invest New Drugs* 2000; **18**: 95–107.
38 Ewald B, Sampath D, Plunkett W. H2AX phosphorylation marks gemcitabine-induced stalled replication forks and their collapse upon S-phase checkpoint abrogation. *Mol Cancer Ther* 2007; **6**: 1239–48.
39 Kohn EA, Yoo CJ, Eastman A. The protein kinase C inhibitor Go6976 is a potent inhibitor of DNA damage-induced S and G2 cell cycle checkpoints. *Cancer Res* 2003; **63**: 31–5.
40 Semenza GL. Targeting HIF-1 for cancer therapy. *Nat Rev Cancer* 2003; **3**: 721–32.
41 Koukourakis MI, Giatromanolaki A, Sivridis E *et al.* Hypoxia-inducible factor (HIF1A and HIF2A), angiogenesis, and chemoradiotherapy outcome of squamous cell head-and-neck cancer. *Int J Radiat Oncol Biol Phys* 2002; **53**: 1192–202.
42 Chen EY, Mazure NM, Cooper JA, Giaccia AJ. Hypoxia activates a platelet-derived growth factor receptor/phosphatidylinositol 3-kinase/Akt pathway that results in glycogen synthase kinase-3 inactivation. *Cancer Res* 2001; **61**: 2429–33.
43 Esumi H, Izuishi K, Kato K *et al.* Hypoxia and nitric oxide treatment confer tolerance to glucose starvation in a 5'-AMP-activated protein kinase-dependent manner. *J Biol Chem* 2002; **277**: 32791–8.
44 Bonner WM, Redon CE, Dickey JS *et al.* GammaH2AX and cancer. *Nat Rev Cancer* 2008; **8**: 957–67.
45 Tse AN, Carvajal R, Schwartz GK. Targeting checkpoint kinase 1 in cancer therapeutics. *Clin Cancer Res* 2007; **13**: 1955–60.
46 Ewald B, Sampath D, Plunkett W. ATM and the Mre11-Rad50-Nbs1 complex respond to nucleoside analogue-induced stalled replication forks and contribute to drug resistance. *Cancer Res* 2008; **68**: 7947–55.
47 Parsels LA, Morgan MA, Tanska DM *et al.* Gemcitabine sensitization by checkpoint kinase 1 inhibition correlates with inhibition of a Rad51 DNA damage response in pancreatic cancer cells. *Mol Cancer Ther* 2009; **8**: 45–54.

48 Chan N, Koritzinsky M, Zhao H *et al.* Chronic hypoxia decreases synthesis of homologous recombination proteins to offset chemoresistance and radioresistance. *Cancer Res* 2008; **68**: 605–14.
49 Bristow RG, Hill RP. Hypoxia and metabolism Hypoxia, DNA repair and genetic instability. *Nat Rev Cancer* 2008; **8**: 180–92.
50 Skladanowski A, Bozko P, Sabisz M, Larsen AK. Dual inhibition of PI3K/Akt signaling and the DNA damage checkpoint in p53-deficient cells with strong survival signaling: implications for cancer therapy. *Cell Cycle* 2007; **6**: 2268–75.
51 Morgan MA, Parsels LA, Parsels JD, Mesiwala AK, Maybaum J, Lawrence TS. Role of checkpoint kinase 1 in preventing premature mitosis in response to gemcitabine. *Cancer Res* 2005; **65**: 6835–42.
52 Morgan MA, Parsels LA, Parsels JD, Lawrence TS, Maybaum J. The relationship of premature mitosis to cytotoxicity in response to checkpoint abrogation and antimetabolite treatment. *Cell Cycle* 2006; **5**: 1983–8.
53 Matthews DJ, Yakes FM, Chen J *et al.* Pharmacological abrogation of S-phase checkpoint enhances the anti-tumor activity of gemcitabine in vivo. *Cell Cycle* 2007; **6**: 104–10.
54 Karnitz LM, Flatten KS, Wagner JM *et al.* Gemcitabine-induced activation of checkpoint signaling pathways that affect tumor cell survival. *Mol Pharmacol* 2005; **68**: 1636–44.
55 Pham NA, Tsao MS, Cao P, Hedley DW. Dissociation of gemcitabine sensitivity and protein kinase B signaling in pancreatic ductal adenocarcinoma models. *Pancreas* 2007; **35**: e16–26.
56 Klein JB, Barati MT, Wu R *et al.* Akt-mediated valosin-containing protein 97 phosphorylation regulates its association with ubiquitinated proteins. *J Biol Chem* 2005; **280**: 31870–81.
57 Yokoi K, Fidler IJ. Hypoxia increases resistance of human pancreatic cancer cells to apoptosis induced by gemcitabine. *Clin Cancer Res* 2004; **10**: 2299–306.
58 Shi Z, Azuma A, Sampath D, Li YX, Huang P, Plunkett W. S-Phase arrest by nucleoside analogues and abrogation of survival without cell cycle progression by 7-hydroxystaurosporine. *Cancer Res* 2001; **61**: 1065–72.
59 Cheng JQ, Ruggeri B, Klein WM *et al.* Amplification of AKT2 in human pancreatic cells and inhibition of AKT2 expression and tumorigenicity by antisense RNA. *Proc Natl Acad Sci U S A* 1996; **93**: 3636–41.
60 Ruggeri BA, Huang L, Wood M, Cheng JQ, Testa JR. Amplification and overexpression of the AKT2 oncogene in a subset of human pancreatic ductal adenocarcinomas. *Mol Carcinog* 1998; **21**: 81–6.
61 Izuishi K, Kato K, Ogura T, Kinoshita T, Esumi H. Remarkable tolerance of tumor cells to nutrient deprivation: possible new biochemical target for cancer therapy. *Cancer Res* 2000; **60**: 6201–7.

doi: 10.1111/j.1349-7006.2011.01880.x

Journal of Controlled Release 149 (2011) 36–41

Contents lists available at ScienceDirect

Journal of Controlled Release

journal homepage: www.elsevier.com/locate/jconrel

Review

Progress in the development of ultrasound-mediated gene delivery systems utilizing nano- and microbubbles

Ryo Suzuki, Yusuke Oda, Naoki Utoguchi, Kazuo Maruyama *

Department of Biopharmaceutics, School of Pharmaceutical Sciences, Teikyo University, 1091-1 Suwarashi, Midori-ku, Sagamihara, Kanagawa 252-5195, Japan

ARTICLE INFO

Article history:
Received 28 December 2009
Accepted 6 May 2010
Available online 12 May 2010

Keywords:
Ultrasound
Microbubbles
Sonoporation
Gene delivery
Cavitation

ABSTRACT

Recently, ultrasound-mediated gene delivery with nano- and microbubbles was developed as a novel non-viral vector system. In this gene delivery system, microstreams and microjets, which are induced by disruption of nano/microbubbles exposed to ultrasound, are used as the driving force to transfer genes into cells by opening transient pores in the cell membrane. This system can directly deliver plasmid DNA and siRNA into cytosol without endocytosis pathway. Therefore, these genes are able to escape from degradation in lysosome and result in enhancing the efficiency of gene expression. In addition, it is expected that ultrasound-mediated gene delivery using nano/microbubbles would be a system to establish non-invasive and tissue specific gene expression because ultrasound can transdermally expose to target tissues and organs. This review focuses on the current ultrasound-mediated gene delivery system using nano/microbubbles. We discuss about the feasibility of this gene delivery system as novel non-viral vector system.

Contents

1. Introduction

Gene therapy has a potential in the treatment of cancer and diseases that are due to genomic causes. Viral vectors are efficient carriers of genes for transduction, but some problems have become evident [1–3]. Delivery vectors that are highly potent in terms of gene transduction efficiency should also be safe and easy to apply. Non-viral vectors have recently received focus as gene carriers, but their transduction efficiency is very low. Efforts have recently been directed towards improving this aspect [4–6]. Towards this end, ultrasound has been investigated for improving the efficiency of transgene delivery, and holds promise as a non-invasive gene delivery system.

Ultrasound shows potential for improving the efficiency of gene delivery into tissues and cells, a technique known as sonophoresis/sonoporation [7]. It is believed that ultrasound perturbs cell membranes and causes transient pores to open in the membrane, thus facilitating gene entry into the cell [8]. In addition, it has been reported that microbubbles utilized as ultrasound contrast agents play an important role in enhancing the efficiency of gene delivery, without causing cell damage [9]. In general, cell damage is dependent on ultrasound intensity, concentration of microbubbles and cell type. Especially, ultrasound intensity and exposure time are key factors. Therefore, it is important to optimize the condition of ultrasound exposure in ultrasound-mediated gene delivery [10–13]. Some researchers studied about the cell damage by the disruption of microbubbles with ultrasound exposure [14–19]. These reports are useful as informative references for ultrasound-mediated gene delivery utilizing microbubbles.

* Corresponding author. Tel.: +81 42 685 3722; fax: +81 42 685 3432.
E-mail address: maruyama@pharm.teikyo-u.ac.jp (K. Maruyama).

0168-3659/$ – see front matter
doi:10.1016/j.jconrel.2010.05.009

Microbubbles which are destroyed by ultrasound exposure generate microstreams or microjets, resulting in shear stress to cells and the generation of transient holes in cell membranes [20]. Since this approach can be used to deliver extracellular molecules such as genes into cells, microbubbles could facilitate ultrasound-mediated gene delivery. In addition, submicron sized bubbles (nanobubbles), which are smaller than conventional microbubbles, were recently reported [21,22], and we have also developed novel liposomal nanobubbles (Bubble liposomes) [11,23–32]. These nanobubbles can also be utilized as enhancing tool of gene delivery efficiency in ultrasound-mediated gene delivery. In this review, we introduced about ultrasound-mediated delivery systems combined with nano/microbubbles and discussed the feasibility as non-viral vector system.

2. Microbubbles as ultrasound contrast agents

Ultrasonography is a widely used diagnostic medical imaging technique that is non-invasive, relatively low-cost, easy to use, provides real-time imaging, and importantly, avoids the use of hazardous ionizing radiation. Ultrasound wave pulses generated by an ultrasound transducer are partially reflected or scattered by the interfaces between different tissues. The transducer detects the ultrasound waves returned by scattering, and these signals are converted to ultrasound images. Since blood scatters ultrasound poorly, ultrasound contrast agents, which increase the scattering and reflection of ultrasound waves, are utilized for blood flow imaging, especially in cardiosonography. Gramiak and Shah in 1968 were the first to use contrast agents in echocardiography [33], and reported that the aortic delineation was improved by intracardiac injection of agitated saline containing air bubbles. However, these air microspheres disappeared within a few seconds following intravenous injection due to the high solubility of air in blood, and the impossibility of larger air bubbles to pass through pulmonary capillaries. For these reasons, it is difficult to use injected conventional air bubbles for opacifying the left cardiac chambers, unless they are injected by the intracoronary or aortic route.

To improve the stability and decrease the size of air bubbles, microbubbles with a thin shell such as albumin (Albunex) or galactose palmitic acid (Levovist) have been developed (Table 1). These bubbles are first-generation microbubbles, and are air-filled microspheres. Their mean diameter ranges from 1 to 8 μm, and they are capable of passing through pulmonary capillaries. However, these air-filled microbubbles disappear from the bloodstream within seconds after administration because of their low resistance to arterial pressure gradients, and the high solubility of air in blood [34]. Approaches for increasing the stability of microbubbles and decreasing the solubility of their gas in blood are clearly required, and lead to the development of microbubbles filled with a high molecular weight hydrophobic gas such as perfluorocarbons or sulfur hexafluoride. These microbubbles represent second-generation contrast agents, in which surfactants, sonicated albumin and phospholipids are used to form the bubble shell in order to improve microbubble stability in the bloodstream. The acoustic backscatter of these microbubbles is higher than that of blood and organs, due to differences in acoustic impedance between gases, and blood or organs. Therefore, microbubbles are useful contrast agents, especially in echocardiography. In addition, Sonazoid which was a phosphatidylserine-stabilized perfluorobutane microbubbles was developed as a useful contrast agent for hepatic tumors [35–37]. This is due to uniqueness of Sonazoid whose microbubbles are likely to be taken up by Kupffer cells (liver macrophages) in the healthy liver and enhances contrast of the liver parenchyma during the delayed phase, which usually occurs within 10 min after the injection. In contrast, tumor that lacks Kupffer cells was not enhanced resulting in clear negative contrast of the tumor [36]. Thus, Sonazoid is a new type of microbubble which is able to target Kupffer cells. However, Sonazoid has been commercially available microbubble for clinical use only in Japan since 2007. In the future, it is expected that tissue specific targeting bubbles such as Sonazoid are developed.

Table 1
Ultrasound contrast agents.

Name	Shell	Entrapping gas	Size (μm)
Albunex	Albumin	Air	4.3
Levovist	Galactose	Air	2–4
Optison	Albumin	Perfluoropropane	3–32
Definity	Lipids	Perfluoropropane	1.1–20
Imagent	Lipids	Perfluoropropane	5
Sonovue	Lipids	Sulphur hexafluoride	2.5
Sonazoid	Lipids	Perfluorobutane	2–3

3. Properties of microbubbles combined with ultrasound

The behavior of microbubbles depends on the amplitude of ultrasound used. At very low acoustic pressure (mechanical index (MI)<0.05–0.1), the microbubbles cause linear oscillation, and the reflected frequency is equal to the transmitted frequency (Fig. 1(a)). An increase in acoustic pressure (0.1<MI<0.3), referred to as low-power imaging, causes non-linear expansion and compression of the microbubbles (Fig. 1(b)). In fact, the bubble becomes somewhat more resistant to compression than to expansion. This phenomenon is known as stable or non-inertial cavitation, and results in the emission of non-linear harmonic signals at multiples of the transmitted frequency [38]. Harmonic imaging with microbubbles enhances the bubbles-to-tissue backscatter signal ratio, due to insignificant harmonic backscatter from tissue in this range of MI. Therefore, this technique can improve the signal-noise ratio and be useful in left ventricular pacification imaging [39]. In addition, stable or non-inertial cavitation can enhance transient cell membrane permeability (Fig. 2(a)) [40]. Machluf et al. reported that ultrasound exposure (0.16 MI, 1 MHz) in the presence of microbubbles deliver plasmid DNA into cells [41,42].

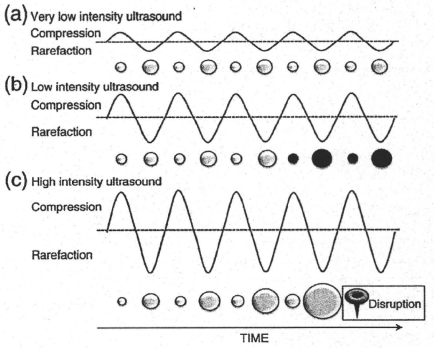

Fig. 1. Scheme showing microbubble behavior in acoustic fields (a) Very low intensity ultrasound induces linear oscillation of the microbubble. (b) Low intensity ultrasound induces oscillation of the microbubble with a gradual increase in microbubble diameter until it reaches a resonant diameter, at which point stable oscillation occurs (filled black circles). (c) High intensity ultrasound causes a rapid increase in the diameter of the microbubble for a few cycles, which induces bubble disruption.

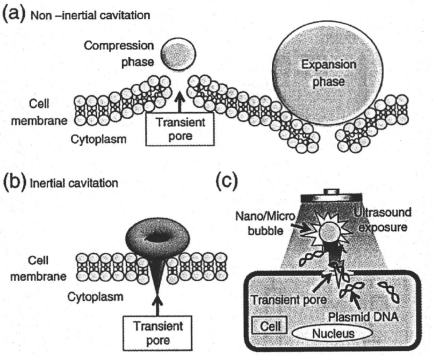

Fig. 2. Scheme showing the pore formation in the cell membrane by oscillating or disrupting microbubble (a) The pushing and pulling behavior (non-inertial cavitation) of the microbubble and (b) the collapse of microbubbles (inertial cavitation) cause rupture of the cell membrane creating pore allowing trans-membrane flux of fluid and macromolecules such as plasmid DNA and oligonucleotides (c).

Higher acoustic pressure (MI>0.3–0.6) causes forced expansion and compression of microbubbles and results in bubble disruption (collapse) (Fig. 1(c)). This inertial cavitation involved in bubble disruption is utilized as flash-replenishment in reperfusion study of diagnosis [43]. This inertial cavitation induces microstreams/microjets around the bubbles. The peak velocity of the microstreams/microjets can reach 700 m/s. These microstreams/microjets can enhance the permeability of cell membranes due to the formation of transient pores (Fig. 2(b)) [20]. In the presence of nano-/microbubbles, the threshold for cavitation decreases, and it results in rendering their destruction feasible at lower energies of ultrasound.

4. Gene delivery using sonoporation as a non-viral vector system

The first studies investigating the utility of ultrasound for gene delivery used frequencies in the range 20–50 kHz [7,44]. However, these frequencies, along with cavitation, are known to cause tissue damage if not properly controlled [45,46]. To overcome this problem, many gene delivery studies have used therapeutic ultrasound, which operates at frequencies of 1–3 MHz, intensities of 0.5–2.5 W/cm^2 or MI 0.3–2, and in pulse-mode [47]. However, as these conditions result in very inefficient gene delivery, therapeutic ultrasound combined with nano/microbubble contrast agents has been investigated for enhancing gene transfection efficiency [9,13,48,49]. This combination method has many of the characteristics required for practical gene therapy including low toxicity, the potential for repeated applications, organ specificity and broad applicability to acoustically accessible organs. Under proper conditions, the combination of ultrasound and nano/microbubbles can create transient non-lethal perforations in cell membranes. Taniyama et al. reported that transient pores formed in cell membranes upon exposure to ultrasound and Optison, and that the pores completely closed [20]. In addition, the behavior of insonated microbubbles was observed with high-speed camera microscopy [50]. Exposure to high intensity ultrasound induced complete disruption of the microbubbles. The above findings suggest that the combination of microbubbles and ultrasound could be useful for gene delivery (Fig. 2(c)).

4.1. Applying to plasmid DNA delivery

Much research has been conducted both *in vitro* and *in vivo* into gene delivery using ultrasound to disrupt microbubbles. In early feasibility studies, reporter genes such as luciferase, β-galactosidase and green fluorescent protein (GFP) were utilized to assess transfection efficiency [13,51–54]. Transfection method in *in vitro* study is very simple. In general, cells suspended with microbubbles and plasmid DNA were exposed with ultrasound for a few second-several tens of seconds due to be completed transfection in a short period of time [27]. Transfection efficiency is affected by ultrasound exposure condition such as intensity, frequency, period, duty cycle, or type and concentration of microbubble [10,11,13,14]. Normally, the efficiency increase according to increasing ultrasound intensity and period [11]. On the other hand, it was reported that the efficiency and cell viability by the transfection with fractionated exposure was higher than that with continuous exposure in the same period of total exposure [19]. In addition, it was reported that there was optimal concentration of microbubbles [55]. Unfortunately, optimal condition is not completely clear in the transfection using this system because of many changeable parameters as mentioned above. Thus, some researchers have studies the properties of this transfection technology to find out optimal condition.

Many of *in vivo* early studies focused on organs and tissues that are readily imaged by diagnostic ultrasonography, including heart [52,56], skeletal muscle [51] and kidney [57]. Bekeredjian et al. reported the use of ultrasound and microbubbles to deliver reporter genes into heart [56]. Subsequently, Korpanty et al. succeeded in delivering the gene for vascular endothelial growth factor (VEGF) into heart using the same gene delivery system, and VEGF-mediated angiogenesis to rat myocardium [58]. This technique has begun to be broadly utilized as a gene delivery system to other organs, tissues and cells such as the vascular system, pancreas, central nerve system, tumors, and hematopoietic cells. For example, Shimamura et al. reported transfection to the central nervous system by sonoporation after injection of a reporter gene and Optison into cistern magna or striatum [59]. In this study, transfection by microbubbles using ultrasound transferred the reporter gene into cells around the neurons, and not into the neuron cells themselves. Takahashi et al. reported gene transfer into the spine using ultrasound and microbubbles [60]. In addition, Aoi et al. developed herpes simplex virus mediated thymidine kinase (HSV-tk)-mediated suicide gene therapy using nanobubbles and ultrasound [61]. In this therapy, HSV-tk corded plasmid DNA and nanobubbles were injected into tumor tissue of mice, and ultrasound was transdermally exposed toward the tissue. The reduction of tumor size was observed by administration of ganciclovir in the mice transfected HSV-tk corded plasmid DNA with nanobubbles and ultrasound. Previously, we developed novel liposomal nanobubble (Bubble liposome) entrapping perfluoropropane gas (Fig. 3(a–c)) [11,27]. The size of Bubble liposomes was about 500 nm and they were much smaller than Sonazoid (Fig. 3(b)). Bubble liposome could also utilize as an effective plasmid DNA delivery tool *in vitro* (Fig. 3(d)) and *in vivo* by the combination with ultrasound. We reported the utility of Bubble liposome in cancer gene therapy using interleukin-12 (IL-12) corded plasmid DNA [24]. The combination of Bubble liposomes and ultrasound dramatically suppressed tumor growth (Fig. 4). As mentioned above, sonoporation combined with nano/microbubbles could be a good system for plasmid DNA delivery.

4.2. Applying to oligonucleotide delivery

Oligonucleotides such as antisense, decoy and small interfering RNA (siRNA) are important molecules that can stop the expression of specific genes [62,63]. In particular, RNA interference (RNAi) using siRNA has potential in the development of new treatments for disease,

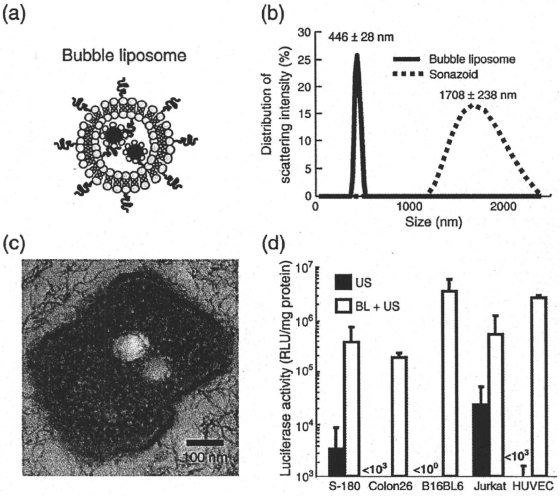

Fig. 3. Comparison of microbubbles and Bubble liposomes (a) Schematic of Bubble liposome. (b) Size distribution of Sonazoid and Bubble liposomes as measured by dynamic light scattering. (c) Transmission electron microscopy (50,000×) of Bubble liposome. (d) Luciferase expression in various types of cells transfected using Bubble liposomes and ultrasound. Cells (1×10^5 cells/500 μL) mixed with pCMV-Luc (5 μg) and Bubble liposomes (60 μg) were exposed or not to ultrasound (frequency, 2 MHz; duty, 50%; burst rate, 2 Hz; intensity, 2.5 W/cm^2; time 10 s). The cells were washed and cultured for 2 days. Thereafter, luciferase activity was determined with luminometer. Data are shown as means ± S.D. ($n=3$). BL, Bubble liposome, pCMV-Luc: luciferase corded plasmid DNA, HUVEC: human umbilical vascular endothelial cell.

including malignant, infectious and autoimmune diseases. In order to achieve efficient gene silencing, it is important that the siRNA is introduced into the cytoplasm of the target cell [64]. Diverse approaches have been attempted to develop efficient oligonucleotide delivery methods [62]. However, technologies that enable the tissue-targeted delivery of siRNA using non-viral vectors need improvement.

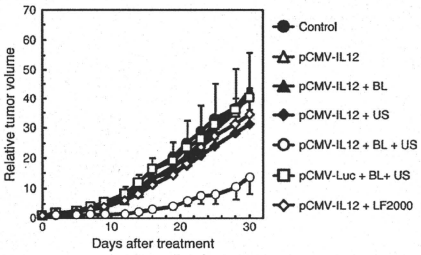

Fig. 4. Cancer gene therapy by IL-12 gene delivery with Bubble liposomes and ultrasound B6C3F1 mice were intradermally inoculated with 1×10^6 OV-HM cells into the flank. On day 7 after tumor inoculation, the tumors were injected with pCMV-IL12 (10 μg) using Bubble liposomes (2.5 μg) and/or ultrasound (1 MHz, 0.7 W/cm^2, 1 min), or Lipofectamine 2000 as a conventional lipofection method. (b) Therapeutic effect was assessed by measuring tumor growth. The volume of the growing tumors was calculated by: (tumor volume; mm^3) = (major axis; mm) × (minor axis; mm)^2 × 0.5). The data are represented as tumor volume relative to the tumor volume on day 7 after tumor inoculation. Each point represents the mean ± SD ($n=5$). BL: Bubble liposomes, US: Ultrasound, LF2000: Lipofectamine 2000, pCMV-IL-12: IL-12 corded plasmid DNA, pCMV-Luc: Luciferase corded plasmid DNA.

As mentioned above, the combination of ultrasound and nano/microbubbles can directly deliver extracellular molecules into the cytosol [25], where antisense, decoy and siRNA function, so this delivery system might better exhibit the functions of these oligonucleotides. Azuma et al. reported that NF-κB decoy delivery into transplanted kidney by the combination of microbubbles and ultrasound could significantly decrease IL-1β and TNF-α (inflammatory cytokines) and prolonged the survival rate of kidney-transplanted mice [57]. Negishi et al. reported that siRNA was directly introduced into the cytoplasm by nanobubbles and ultrasound [30]. In addition, transfection of siRNA into tibialis muscles with nanobubble and ultrasound resulted in gene-silencing, which was sustained for more than 3 weeks. It therefore appears that the combination of nano/microbubbles and ultrasound could be a useful siRNA delivery system. In addition, siRNA transfection with ultrasound and microbubbles was utilized to apply to mesenchymal stem cells, indicating that this technique could be applicable to genetically modified stem cell therapy. Vandenbroucke et al. also developed an interesting siRNA delivery system using sonoporation [65]. They coupled (PEG-siPlex) of PEGylated cationic liposomes and siRNA, and introduced the complex into gas-filled lipid microbubbles. Both the microbubbles and PEG-siPlex, which were modified with biotin, were attached via avidin. Although PEG-siPlex can protect siRNA from digestion by nucleases *in vivo*, PEGylation makes it difficult for the siRNA to be recognized and taken up by the target cells. The microbubble/sonication system should be able to overcome the negative effects of PEGylating siRNA-cationic liposomes (siPlex) and enhance the efficiency of ultrasound-assisted siRNA delivery. Although siRNA delivery mediated by ultrasound and nano/microbubbles must be optimized, this system may open up new perspectives for ultrasound-controlled *in vivo* siRNA delivery.

5. Efforts to tissue- or organ-selective gene delivery

To establish ideal gene therapy, it is important to deliver therapeutic gene into target tissue or organ. In the early study, gene and nano/microbubbles were directly injected into target tissue and organ [53,66]. However, in this method, there are some limitations such as injection volume and injection technique. To improve these problems, some researchers recently developed ultrasound-mediated gene delivery by the supplying gene and nano/microbubbles via blood flow [11,67]. In this delivery, gene expression was limited in the area exposed ultrasound. Ultrasound can be easily focused to a target tissue or organ. Therefore, it might be possible to develop an optimal tissue- or organ-specific gene delivery system by combining nano/microbubble targeting and focused ultrasound. Shen et al. succeeded to developed ultrasound-mediated gene expression in liver via intraportal injection of plasmid DNA and microbubbles [68]. Grayburn et al. reported insulin expression following insulin gene delivery to pancreatic islets in rat by a combination of microbubbles and ultrasound exposure and succeeded to decrease blood glucose level in diabetes rat [67,69]. We also developed the gene delivery into tumor tissue by the combination of injection from tumor dominant artery and ultrasound exposure toward tumor tissue [11]. In addition, transdermal ultrasound exposure toward liver could induce liver selective gene expression after systemic injection of plasmid DNA and Bubble liposomes. In this case, luciferase expression was dominantly observed in the parenchymal cells of liver. These results suggested that Bubble liposomes could quickly transduce plasmid DNA into each tissue by cavitation even under the existence of blood stream. Moreover, we developed the combination method using mannosylated lipoplexes and Bubble liposomes with ultrasound to enhance gene transfection in mannose receptor-expressing cells in liver [29]. In this study, after systemic injection of mannosylated lipoplex, Bubble liposomes were systemically injected and ultrasound was transdermally exposed toward liver. Gene expression was observed mannose receptor-expressing cells such as macrophage and dendritic cells which were known as antigen presenting cells. It is expected that ultrasound-mediated gene delivery with nano/microbubbles might be useful to develop target tissue or organ-selective gene delivery in vivo.

Previously, several groups have reported active targetable nano/microbubbles to endothelium [70], rejected tissues [71], neovasculature endothelium [72], lymph node-related vasculature [73] and activated platelets[74] by targeting ICAM-1 [75], VCAM-1 [76] or integrins [77]. We also developed blood clot targetable Bubble liposomes modified with arginine-glycine-aspartic acid (RGD) peptides to develop effective ultrasound contrast agents for blood clots imaging [78]. Although these nano/microbubbles were developed as ultrasound imaging agents, it might be possible to develop an optimal tissue- or organ-selective gene delivery system by combining targetable nano/microbubble associated with gene and ultrasound.

6. Conclusion

Ultrasound has long been utilized as a useful diagnostic tool. Therapeutic ultrasound was recently developed and is being utilized in clinical settings. The combination of therapeutic ultrasound and nano/microbubbles is an interesting and important system for establishing a novel and non-invasive gene delivery system. Gene expression efficiency with this system can effectively deliver gene compared with conventional non-viral vector system such as lipofection method due to deliver gene into cytosol without endocytosis pathway. Many *in vivo* studies has been reported about ultrasound-mediated gene delivery with nano/microbubbles. Especially, there are some reports about feasibility studies of gene therapy for various diseases [24,29,61,67] In addition, this system has a potency of site specific gene delivery by the control of ultrasound exposure site. Therefore, it is expected that this technology would be utilized as a novel gene delivery system in clinical field.

References

[1] E. Check, Safety panel backs principle of gene-therapy trials, Nature 420 (2002) 595.
[2] E. Check, Second cancer case halts gene-therapy trials, Nature 421 (2003) 305.
[3] E. Marshall, Gene therapy death prompts review of adenovirus vector Science 286 (1999) 2244–2245.
[4] K. Kogure, H. Akita, Y. Yamada, H. Harashima, Multifunctional envelope-type nano device (MEND) as a non-viral gene delivery system, Adv. Drug Deliv. Rev. 60 (2008) 559–571.
[5] F. Liu, C.C. Conwell, X. Yuan, L.M. Shollenberger, L. Huang, Novel nonviral vectors target cellular signaling pathways: regulated gene expression and reduced toxicity, J. Pharmacol. Exp. Ther. 321 (2007) 777–783.
[6] K. Itaka, S. Ohba, K. Miyata, H. Kawaguchi, K. Nakamura, T. Takato, U.I. Chung, K. Kataoka, Bone regeneration by regulated in vivo gene transfer using biocompatible polyplex nanomicelles, Mol. Ther. 15 (2007) 1655–1662.
[7] M. Fechheimer, J.F. Boylan, S. Parker, J.E. Sisken, G.L. Patel, S.G. Zimmer, Transfection of mammalian cells with plasmid DNA by scrape loading and sonication loading, Proc. Natl. Acad. Sci. U. S. A. 84 (1987) 8463–8467.
[8] M.W. Miller, D.L. Miller, A.A. Brayman, A review of in vitro bioeffects of inertial ultrasonic cavitation from a mechanistic perspective, Ultrasound Med. Biol. 22 (1996) 1131–1154.
[9] W.J. Greenleaf, M.E. Bolander, G. Sarkar, M.B. Goldring, J.F. Greenleaf, Artificial cavitation nuclei significantly enhance acoustically induced cell transfection, Ultrasound Med. Biol. 24 (1998) 587–595.
[10] L.B. Feril Jr., R. Ogawa, K. Tachibana, T. Kondo, Optimized ultrasound-mediated gene transfection in cancer cells, Cancer Sci. 97 (2006) 1111–1114.
[11] R. Suzuki, T. Takizawa, Y. Negishi, N. Utoguchi, K. Sawamura, K. Tanaka, E. Namai, Y. Oda, Y. Matsumura, K. Maruyama, Tumor specific ultrasound enhanced gene transfer in vivo with novel liposomal bubbles, J. Control. Release 125 (2008) 137–144.
[12] S.V. Pislaru, C. Pislaru, R.R. Kinnick, R. Singh, R. Gulati, J.F. Greenleaf, R.D. Simari, Optimization of ultrasound-mediated gene transfer: comparison of contrast agents and ultrasound modalities, Eur. Heart J. 24 (2003) 1690–1698.
[13] T. Li, K. Tachibana, M. Kuroki, M. Kuroki, Gene transfer with echo-enhanced contrast agents: comparison between Albunex, Optison, and Levovist in mice–initial results, Radiology 229 (2003) 423–428.
[14] M.A. Hassan, M.A. Buldakov, R. Ogawa, Q.L. Zhao, Y. Furusawa, N. Kudo, T. Kondo, P. Riesz, Modulation control over ultrasound-mediated gene delivery: evaluating the importance of standing waves, J. Control. Release 141 (2010) 70–76.
[15] D.J. Wells, Electroporation and ultrasound enhanced non-viral gene delivery in vitro and in vivo, Cell Biol. Toxicol. 26 (2010) 21–28.
[16] M.A. Hassan, L.B. Feril Jr., K. Suzuki, N. Kudo, K. Tachibana, T. Kondo, Evaluation and comparison of three novel microbubbles: enhancement of ultrasound-induced cell death and free radicals production, Ultrason. Sonochem. 16 (2009) 372–378.
[17] L.B. Feril Jr., T. Kondo, Q.L. Zhao, R. Ogawa, K. Tachibana, N. Kudo, S. Fujimoto, S. Nakamura, Enhancement of ultrasound-induced apoptosis and cell lysis by echo-contrast agents, Ultrasound Med. Biol. 29 (2003) 331–337.
[18] N. Kudo, K. Okada, K. Yamamoto, Sonoporation by single-shot pulsed ultrasound with microbubbles adjacent to cells, Biophys. J. 96 (2009) 4866–4876.
[19] D.P. Guo, X.Y. Li, P. Sun, Y.B. Tang, X.V. Chen, Q. Chen, L.M. Fan, B. Zang, L.Z. Shao, X.R. Li, Ultrasound-targeted microbubble destruction improves the low density lipoprotein receptor gene expression in HepG2 cells, Biochem. Biophys. Res. Commun. 343 (2006) 470–474.
[20] Y. Taniyama, K. Tachibana, K. Hiraoka, T. Namba, K. Yamasaki, N. Hashiya, M. Aoki, T. Ogihara, K. Yasufumi, R. Morishita, Local delivery of plasmid DNA into rat carotid artery using ultrasound, Circulation 105 (2002) 1233–1239.
[21] Z. Gao, A.M. Kennedy, D.A. Christensen, N.Y. Rapoport, Drug-loaded nano/microbubbles for combining ultrasonography and targeted chemotherapy, Ultrasonics 48 (2008) 260–270.
[22] Y. Wang, X. Li, Y. Zhou, P. Huang, Y. Xu, Preparation of nanobubbles for ultrasound imaging and intracelluar drug delivery, Int. J. Pharm. 384 (2010) 148–153.
[23] R. Suzuki, K. Maruyama, Effective in vitro and in vivo gene delivery by the combination of liposomal bubbles (bubble liposomes) and ultrasound exposure, Methods Mol. Biol. 605 (2009) 473–486.
[24] R. Suzuki, E. Namai, Y. Oda, N. Nishiie, S. Otake, R. Koshima, K. Hirata, Y. Taira, N. Utoguchi, Y. Negishi, S. Nakagawa, K. Maruyama, Cancer gene therapy by IL-12 gene delivery using liposomal bubbles and tumoral ultrasound exposure, J. Control. Release 142 (2010) 245–250.
[25] R. Suzuki, Y. Oda, N. Utoguchi, E. Namai, Y. Taira, N. Okada, N. Kadowaki, T. Kodama, K. Tachibana, K. Maruyama, A novel strategy utilizing ultrasound for antigen delivery in dendritic cell-based cancer immunotherapy, J. Control. Release 133 (2009) 198–205.
[26] R. Suzuki, T. Takizawa, Y. Kuwata, M. Mutoh, N. Ishiguro, N. Utoguchi, A. Shinohara, M. Eriguchi, H. Yanagie, K. Maruyama, Effective anti-tumor activity of oxaliplatin encapsulated in transferrin-PEG-liposome, Int. J. Pharm. 346 (2008) 143–150.
[27] R. Suzuki, T. Takizawa, Y. Negishi, K. Hagisawa, K. Tanaka, K. Sawamura, N. Utoguchi, T. Nishioka, K. Maruyama, Gene delivery by combination of novel liposomal bubbles with perfluoropropane and ultrasound, J. Control. Release 117 (2007) 130–136.
[28] R. Suzuki, T. Takizawa, Y. Negishi, N. Utoguchi, K. Maruyama, Effective gene delivery with liposomal bubbles and ultrasound as novel non-viral system, J. Drug Target. 15 (2007) 531–537.

[29] K. Un, S. Kawakami, R. Suzuki, K. Maruyama, F. Yamashita, M. Hashida, Enhanced transfection efficiency into macrophages and dendritic cells by a combination method using mannosylated lipoplexes and bubble liposomes with ultrasound exposure, Hum. Gene Ther. 21 (2010) 65–74.

[30] Y. Negishi, Y. Endo, T. Fukuyama, R. Suzuki, T. Takizawa, D. Omata, K. Maruyama, Y. Aramaki, Delivery of siRNA into the cytoplasm by liposomal bubbles and ultrasound, J. Control. Release 132 (2008) 124–130.

[31] Y. Negishi, D. Omata, H. Iijima, Y. Takabayashi, K. Suzuki, Y. Endo, R. Suzuki, K. Maruyama, M. Nomizu, Y. Aramaki, Enhanced laminin-derived peptide AG73-mediated liposomal gene transfer by bubble liposomes and ultrasound, Mol. Pharm. 7 (2010) 217–226.

[32] T. Yamashita, S. Sonoda, R. Suzuki, N. Arimura, K. Tachibana, K. Maruyama, T. Sakamoto, A novel bubble liposome and ultrasound-mediated gene transfer to ocular surface: RC-1 cells in vitro and conjunctiva in vivo, Exp. Eye Res . 85 (2007) 741–748.

[33] P.M. Shah, R. Gramiak, D.H. Kramer, P.N. Yu, Determinants of atrial (S4) and ventricular (S3) gallop sounds in primary myocardial disease, N Engl J. Med. 278 (1968) 753–758.

[34] A. Kabalnov, D. Klein, T. Pelura, E. Schutt, J. Weers, Dissolution of multicomponent microbubbles in the bloodstream: 1, Theory Ultrasound Med Biol 24 (1998) 739–749.

[35] K. Yanagisawa, F. Moriyasu, T. Miyahara, M. Yuki, H. Iijima, Phagocytosis of ultrasound contrast agent microbubbles by Kupffer cells, Ultrasound Med. Biol. 33 (2007) 318–325.

[36] R. Watanabe, M. Matsumura, T. Munemasa, M. Fujimaki, M. Suematsu, Mechanism of hepatic parenchyma-specific contrast of microbubble-based contrast agent for ultrasonography: microscopic studies in rat liver, Invest. Radiol. 42 (2007) 643–651.

[37] K. Korenaga, M. Korenaga, M. Furukawa, T. Yamasaki, I. Sakaida, Usefulness of Sonazoid contrast-enhanced ultrasonography for hepatocellular carcinoma: comparison with pathological diagnosis and superparamagnetic iron oxide magnetic resonance images, J. Gastroenterol. 44 (2009) 733–741.

[38] E.C. Unger, E. Hersh, M. Vannan, T.O. Matsunaga, T. McCreery, Local drug and gene delivery through microbubbles, Prog. Cardiovasc. Dis. 44 (2001) 45–54.

[39] S.L. Mulvagh, A.N. DeMaria, S.B. Feinstein, P.N. Burns, S. Kaul, J.G. Miller, M. Monaghan, T.R. Porter, L.J. Shaw, F.S. Villanueva, Contrast echocardiography: current and future applications, J. Am. Soc. Echocardiogr. 13 (2000) 331–342.

[40] A. van Wamel, K. Kooiman, M. Harteveld, M. Emmer, F.J. ten Cate, M. Versluis, N. de Jong, Vibrating microbubbles poking individual cells: drug transfer into cells via sonoporation, J. Control. Release 112 (2006) 149–155.

[41] M. Duvshani-Eshet, L. Baruch, E. Kesselman, E. Shimoni, M. Machluf, Therapeutic ultrasound-mediated DNA to cell and nucleus: bioeffects revealed by confocal and atomic force microscopy, Gene Ther. 13 (2006) 163–172.

[42] M. Duvshani-Eshet, D. Adam, M. Machluf, The effects of albumin-coated microbubbles in DNA delivery mediated by therapeutic ultrasound, J. Control. Release 112 (2006) 156–166.

[43] K. Kalantarinia, J.T. Belcik, J.T. Patrie, K. Wei, Real-time measurement of renal blood flow in healthy subjects using contrast-enhanced ultrasound, Am. J. Physiol. Ren. Physiol 297 (2009) F1129–F1134.

[44] M. Joersbo, J. Brunstedt, Protein synthesis stimulated in sonicated sugar beet cells and protoplasts, Ultrasound Med. Biol. 16 (1990) 719–724.

[45] H.R. Guzman, A.J. McNamara, D.X. Nguyen, M.R. Prausnitz, Bioeffects caused by changes in acoustic cavitation bubble density and cell concentration: a unified explanation based on cell-to-bubble ratio and blast radius, Ultrasound Med. Biol. 29 (2003) 1211–1222.

[46] W. Wei, B. Zheng-zhong, W. Yong-jie, Z. Qing-wu, M. Ya-lin, Bioeffects of low-frequency ultrasonic gene delivery and safety on cell membrane permeability control, J. Ultrasound Med. 23 (2004) 1569–1582.

[47] H.J. Kim, J.F. Greenleaf, R.R. Kinnick, J.T. Bronk, M.E. Bolander, Ultrasound-mediated transfection of mammalian cells, Hum. Gene Ther. 7 (1996) 1339–1346.

[48] D.M. Hallow, A.D. Mahajan, T.E. McCutchen, M.R. Prausnitz, Measurement and correlation of acoustic cavitation with cellular bioeffects, Ultrasound Med. Biol. 32 (2006) 1111–1122.

[49] R.V. Shohet, S. Chen, Y.T. Zhou, Z. Wang, R.S. Meidell, R.H. Unger, P.A. Grayburn, Echocardiographic destruction of albumin microbubbles directs gene delivery to the myocardium, Circulation 101 (2000) 2554–2556.

[50] A. van Wamel, A. Bouakaz, M. Versluis, N. de Jong, Micromanipulation of endothelial cells: ultrasound–microbubble-cell interaction, Ultrasound Med. Biol. 30 (2004) 1255–1258.

[51] J.P. Christiansen, B.A. French, A.L. Klibanov, S. Kaul, J.R. Lindner, Targeted tissue transfection with ultrasound destruction of plasmid-bearing cationic microbubbles, Ultrasound Med. Biol. 29 (2003) 1759–1767.

[52] S. Chen, R.V. Shohet, R. Bekeredjian, P. Frenkel, P.A. Grayburn, Optimization of ultrasound parameters for cardiac gene delivery of adenoviral or plasmid deoxyribonucleic acid by ultrasound-targeted microbubble destruction, J. Am. Coll. Cardiol. 42 (2003) 301–308.

[53] Q.L. Lu, H.D. Liang, T. Partridge, M.J. Blomley, Microbubble ultrasound improves the efficiency of gene transduction in skeletal muscle in vivo with reduced tissue damage, Gene Ther. 10 (2003) 396–405.

[54] S. Tsunoda, O. Mazda, Y. Oda, Y. Iida, S. Akabame, T. Kishida, M. Shin-Ya, H. Asada, S. Gojo, J. Imanishi, H. Matsubara, T. Yoshikawa, Sonoporation using microbubble BR14 promotes pDNA/siRNA transduction to murine heart, Biochem. Biophys. Res. Commun. 336 (2005) 118–127.

[55] Y. Taniyama, K. Tachibana, K. Hiraoka, M. Aoki, S. Yamamoto, K. Matsumoto, T. Nakamura, T. Ogihara, Y. Kaneda, R. Morishita, Development of safe and efficient novel nonviral gene transfer using ultrasound: enhancement of transfection efficiency of naked plasmid DNA in skeletal muscle, Gene Ther. 9 (2002) 372–380.

[56] R. Bekeredjian, S. Chen, P.A. Frenkel, P.A. Grayburn, R.V. Shohet, Ultrasound-targeted microbubble destruction can repeatedly direct highly specific plasmid expression to the heart, Circulation 108 (2003) 1022–1026.

[57] H. Azuma, N. Tomita, Y. Kaneda, H. Koike, T. Ogihara, Y. Katsuoka, R. Morishita, Transfection of NFkappaB-decoy oligodeoxynucleotides using efficient ultrasound-mediated gene transfer into donor kidneys prolonged survival of rat renal allografts, Gene Ther. 10 (2003) 415–425.

[58] G. Korpanty, S. Chen, R.V. Shohet, J. Ding, B. Yang, P.A. Frenkel, P.A. Grayburn, Targeting of VEGF-mediated angiogenesis to rat myocardium using ultrasonic destruction of microbubbles, Gene Ther. 12 (2005) 1305–1312.

[59] M. Shimamura, N. Sato, Y. Taniyama, S. Yamamoto, M. Endoh, H. Kurinami, M. Aoki, T. Ogihara, Y. Kaneda, R. Morishita, Development of efficient plasmid DNA transfer into adult rat central nervous system using microbubble-enhanced ultrasound, Gene Ther. 11 (2004) 1532–1539.

[60] M. Takahashi, K. Kido, A. Aoi, H. Furukawa, M. Ono, T. Kodama, Spinal gene transfer using ultrasound and microbubbles, J. Control. Release 117 (2007) 267–272.

[61] A. Aoi, Y. Watanabe, S. Mori, M. Takahashi, G. Vassaux, T. Kodama, Herpes simplex virus thymidine kinase-mediated suicide gene therapy using nano/microbubbles and ultrasound, Ultrasound Med. Biol. 34 (2008) 425–434.

[62] E. Fattal, G. Barratt, Nanotechnologies and controlled release systems for the delivery of antisense oligonucleotides and small interfering RNA, Br. J. Pharmacol. 157 (2009) 179–194.

[63] S. Kimura, K. Egashira, L. Chen, K. Nakano, E. Iwata, M. Miyagawa, H. Tsujimoto, K. Hara, R. Morishita, K. Sueishi, R. Tominaga, K. Sunagawa, Nanoparticle-mediated delivery of nuclear factor kappaB decoy into lungs ameliorates monocrotaline-induced pulmonary arterial hypertension, Hypertension 53 (2009) 877–883.

[64] K. Tiemann, J.J. Rossi, RNAi-based therapeutics-current status, challenges and prospects EMBO, Mol. Med. 1 (2009) 142–151.

[65] R.E. Vandenbroucke, I. Lentacker, J. Demeester, S.C. De Smedt, N.N. Sanders, Ultrasound assisted siRNA delivery using PEG-siPlex loaded microbubbles, J. Control. Release 126 (2008) 265–273.

[66] C.H. Miao, A.A. Brayman, K.R. Loeb, P. Ye, L. Zhou, P. Mourad, L.A. Crum, Ultrasound enhances gene delivery of human factor IX plasmid, Hum. Gene Ther. 16 (2005) 893–905.

[67] S. Chen, J.H. Ding, R. Bekeredjian, B.Z. Yang, R.V. Shohet, S.A. Johnston, H.E. Hohmeier, C.B. Newgard, P.A. Grayburn, Efficient gene delivery to pancreatic islets with ultrasonic microbubble destruction technology, Proc. Natl. Acad. Sci. U. S. A. 103 (2006) 8469–8474.

[68] Z.P. Shen, A.A. Brayman, L. Chen, C.H. Miao, Ultrasound with microbubbles enhances gene expression of plasmid DNA in the liver via intraportal delivery, Gene Ther. 15 (2008) 1147–1155.

[69] R. Chai, S. Chen, J. Ding, P.A. Grayburn, Efficient, glucose responsive and islet-specific transgene expression by a modified rat insulin promoter, Gene Ther. 16 (2009) 1202–1209.

[70] F.S. Villanueva, R.J. Jankowski, S. Klibanov, M.L. Pina, S.M. Alber, S.C. Watkins, G.H. Brandenburger, W.R. Wagner, Microbubbles targeted to intercellular adhesion molecule-1 bind to activated coronary artery endothelial cells, Circulation 98 (1998) 1–5.

[71] G.E. Weller, E. Lu, M.M. Csikari, A.L. Klibanov, D. Fischer, W.R. Wagner, F.S. Villanueva, Ultrasound imaging of acute cardiac transplant rejection with microbubbles targeted to intercellular adhesion molecule-1, Circulation 108 (2003) 218–224.

[72] D.B. Ellegala, H. Leong-Poi, J.E. Carpenter, A.L. Klibanov, S. Kaul, M.E. Shaffrey, J. Sklenar, J.R. Lindner, Imaging tumor angiogenesis with contrast ultrasound and microbubbles targeted to alpha(v)beta3, Circulation 108 (2003) 336–341.

[73] P. Hauff, M. Reinhardt, A. Briel, N. Debus, M. Schirner, Molecular targeting of lymph nodes with L-selectin ligand-specific US contrast agent: a feasibility study in mice and dogs, Radiology 231 (2004) 667–673.

[74] P.A. Schumann, J.P. Christiansen, R.M. Quigley, T.P. McCreery, R.H. Sweitzer, E.C. Unger, J.R. Lindner, T.O. Matsunaga, Targeted-microbubble binding selectively to GPIIb IIIa receptors of platelet thrombi, Invest. Radiol. 37 (2002) 587–593.

[75] G.E. Weller, F.S. Villanueva, E.M. Tom, W.R. Wagner, Targeted ultrasound contrast agents: in vitro assessment of endothelial dysfunction and multi-targeting to ICAM-1 and sialyl Lewisx, Biotechnol. Bioeng. 92 (2005) 780–788.

[76] C.Z. Behm, B.A. Kaufmann, C. Carr, M. Lankford, J.M. Sanders, C.E. Rose, S. Kaul, J.R. Lindner, Molecular imaging of endothelial vascular cell adhesion molecule-1 expression and inflammatory cell recruitment during vasculogenesis and ischemia-mediated arteriogenesis, Circulation 117 (2008) 2902–2911.

[77] J.R. Lindner, Detection of inflamed plaques with contrast ultrasound, Am. J. Cardiol. 90 (2002) 32L–35L.

[78] K. Hagisawa, N.T., K. Iida, H. Luo, R.J. Siegel, Thrombolysis using low frequency ultrasound with activated platelet targeting bubble liposome in a rabbit iliac artery, Circulation 112 (Sup.II) (2005) 503.

Published OnlineFirst July 14, 2010; DOI:10.1158/0008-5472.CAN-10-0184

Molecular and Cellular Pathobiology

Cancer Research

Circadian Rhythm of Transferrin Receptor 1 Gene Expression Controlled by c-Myc in Colon Cancer–Bearing Mice

Fumiyasu Okazaki[1], Naoya Matsunaga[1], Hiroyuki Okazaki[1], Naoki Utoguchi[2], Ryo Suzuki[2], Kazuo Maruyama[2], Satoru Koyanagi[1], and Shigehiro Ohdo[1]

Abstract

The abundance of cell surface levels of transferrin receptor 1 (TfR1), which regulates the uptake of iron-bound transferring, correlates with the rate of cell proliferation. Because TfR1 expression is higher in cancer cells than in normal cells, it offers a target for cancer therapy. In this study, we found that the expression of TfR1 in mouse colon cancer cells was affected by the circadian organization of the molecular clock. The core circadian oscillator is composed of an autoregulatory transcription-translation feedback loop, in which CLOCK and BMAL1 are positive regulators and the *Period* (*Per*), *Cryptochrome* (*Cry*), and *Dec* genes act as negative regulators. TfR1 in colon cancer–bearing mice exhibited a 24-hour rhythm in mRNA and protein levels. Luciferase reporter analysis and chromatin immunoprecipitation experiments suggested that the clock-controlled gene *c-MYC* rhythmically activated the transcription of the *TfR1* gene. Platinum incorporation into tumor DNA and the antitumor efficacy of transferrin-conjugated liposome-delivered oxaliplatin could be enhanced by drug administration at times when TfR1 expression increased. Our findings suggest that the 24-hour rhythm of TfR1 expression may form an important aspect of strategies for TfR1-targeted cancer therapy. *Cancer Res; 70(15); 6238–46. ©2010 AACR.*

Introduction

In mammals, the master pacemaker controlling the circadian rhythm is located in the suprachiasmatic nuclei of the hypothalamus (1). Regulation of circadian physiology relies on the interplay of interconnected transcription-translation feedback loops. The BMAL1/CLOCK complex activates clock-controlled genes, including *Per, Cry*, and *Dec*, the products of which act as repressors by interacting with BMAL1/CLOCK (2–5). This mechanism also regulates the 24-hour rhythm in output physiology through the periodic activation/repression of clock-controlled output genes in healthy peripheral tissue and tumor tissue (6, 7).

Transferrin receptor 1 (TfR1) is involved in the uptake of iron into cells through the binding and internalization of transferrin, and its regulation by intracellular iron levels has assisted in the elucidation of many important aspects of cellular iron homeostasis (8, 9). Iron is important for metabolism, respiration, and DNA synthesis. Thus, TfR1 is expressed not only in normal healthy cells but also in malignant tumor cells (8, 10). Recently, another TfR-like molecule named TfR2 has been recognized and investigated (11, 12), but the exact function of TfR2 remains unclear (8). It has been reported that the expression of TfR1 in mammary epithelial cells exhibits a significant 24-hour rhythm (13). Such rhythmic variation in TfR1 expression seems to affect its iron uptake function resulting in time-dependent changes in the internalization of iron-loaded Tf. However, it is not clear if the expression of TfR1 in colon cancer cells shows a significant 24-hour rhythm.

Many of the pharmacologic properties of conventional drugs can be improved through the use of an optimized drug delivery system (DDS), which includes particular carriers composed primarily of lipids and/or polymers (14). The high expression of TfR1 in tumor can potentially be used to deliver cytotoxic agents into malignant cells, including chemotherapeutic drugs, cytotoxic proteins (8), and Tf-coupled polyethylene glycol (Tf-PEG) liposomes were designed as intracellular targeting carriers for drugs by systemic administration. In fact, Tf-PEG liposomes encapsulating a platinum (Pt)-based anticancer drug, oxaliplatin, can increase its accumulation in tumor masses (15, 16). On the other hand, daily rhythmic variations in biological functions are thought to affect the efficacy and/or toxicity of drugs: a large number of drugs cannot be expected to have the same potency at different administration times (7, 17). However, it is unclear what influence the rhythmic expression of TfR1 has on the pharmacokinetics/pharmacodynamics of transferrin targeting liposomes.

Authors' Affiliations: [1]Department of Pharmaceutics, Graduate School of Pharmaceutical Sciences, Kyushu University, Fukuoka, Japan and [2]Department of Pharmaceutics, Teikyo University, Sagamiko, Sagamihara, Japan

Note: Supplementary data for this article are available at Cancer Research Online (http://cancerres.aacrjournals.org/).

F. Okazaki, N. Matsunaga, and S. Ohdo contributed equally to this work.

Corresponding Author: Shigehiro Ohdo, Department of Pharmaceutics, Graduate School of Pharmaceutical Sciences, Kyushu University, Fukuoka, 812-8582, Japan. Phone: 81-92-642-6610; Fax: 81-92-642-6614; E-mail: ohdo@phar.kyushu-u.ac.jp.

doi: 10.1158/0008-5472.CAN-10-0184